

國立交通大學

電機與控制工程學系

碩士論文

禪坐之腦電位分佈之微狀態分析
Microstate Analysis of Zen-Meditation Brain
Topography



研究生：李昶毅

指導教授：羅佩禎 教授

中華民國九十七年六月

禪坐之腦電位分佈之微狀態分析

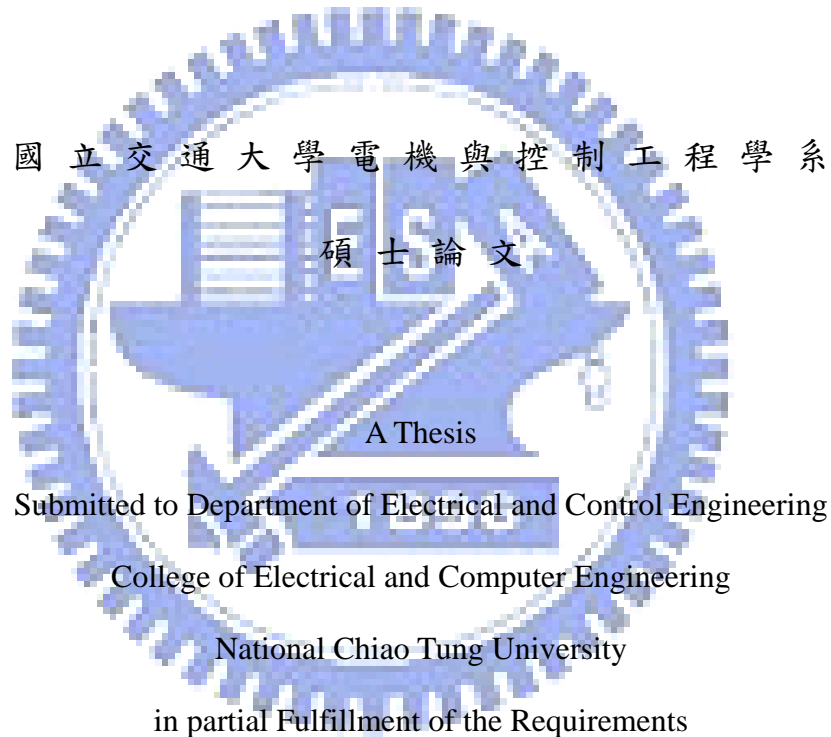
Microstate Analysis of Zen-Meditation Brain Topography

研究生：李昶毅

Student : Chang-Yi Li

指導教授：羅佩禎 教授

Advisor : Dr. Pei-Chen Lo



國立交通大學電機與控制工程學系

碩士論文

A Thesis

Submitted to Department of Electrical and Control Engineering

College of Electrical and Computer Engineering

National Chiao Tung University

in partial Fulfillment of the Requirements

for the Degree of Master

in

Electrical and Control Engineering

June 2008

Hsinchu, Taiwan, Republic of China

中華民國九十七年六月

禪坐之腦電位分佈之微狀態分析

研究生：李昶毅

指導教授：羅佩禎教授

國立交通大學電機與控制工程學系



本篇論文主要目的是提出一套分析腦電波 α 波空間分佈的微狀態的方法，並探討禪坐者與一般人的腦電波在微狀態中的特性及差異性。

首先利用小波分解(wavelet decomposition)和小波重建(wavelet reconstruction)將腦電波中的 α 波頻帶擷取出來，再以各頻帶的能量比例判斷是否為 α 波，並將這 α 波能量計算為一個 30 維度的能量分佈(alpha brain mapping)；接著以馬氏(manalanobis)模糊 C-means(MFCM)最為分類法對各個能量分佈情形進行分類，最後選取特定的分類結果作為狀態分析。

在微狀態分析的結果中發現，在禪坐者的前額 α 波有較長的微狀態維持時間，根據相關的研究認為，微狀態所維持的時間與大腦中資訊處理有相當的關聯，一個較穩定的腦部活動會有較長的微狀態維持時間，也代表在當時有較少的資訊在處理中，視為較為穩定的腦波活動狀態。

Microstate Analysis of Zen-Meditation Brain Topography

Student : Chang-Yi Li

Advisor : Dr. Pei-Chen Lo

Department of Electrical and Control Engineering

National Chiao-Tung University

Abstract

The aim of this study is to propose a method for detecting alpha wave in EEG (electroencephalograph) and analyzing the alpha spatial characteristics in a microstate aspect. We investigated and compared the brain microstates between Zen-meditation practitioners (experimental group) and non-practitioners (control group).

Firstly, EEG epochs of interest were extracted by alpha-power percentage that is at least fifty percent of total power. In the analysis, wavelet decomposition and reconstruction was adopted. Then Mahalanobis Fuzzy C-means clustering was employed in the classification scheme for various alpha mappings. Finally, the alpha-brain microstates were explored and compared for both experimental and control groups.

The preliminary results reveal a longer duration of frontal-alpha microstate observed in Zen-meditation practitioners in comparison with control subjects. From the literatures, a longer duration of microstate may imply that the brain is involved in slight information processing, reflecting a rather stabilized dynamics.

誌謝

首先要感謝我的指導老師羅佩禎老師在這幾年裡對我的教導，也衷心感激老師對於我所付出的耐心，由於老師的認真、嚴謹和親切的態度，讓我受益良多。同時也感謝口試委員楊谷洋老師、陳右穎老師對本論文的指導及建議，讓我知道論文的不足之處，使得論文修正的更加完全。

同時我也要感謝在這兩年內在同一個實驗室的學長姐：致豪、瑄詠、憲正、權毅、適達的殷勤指導。再來感謝我實驗室的同學政恩、恩榮和所有在這裡認識的同學對我的激勵，使我們一起進步成長，也感謝學弟：家鈞、嘉鴻、Bono 陪伴我度過快樂的一年。

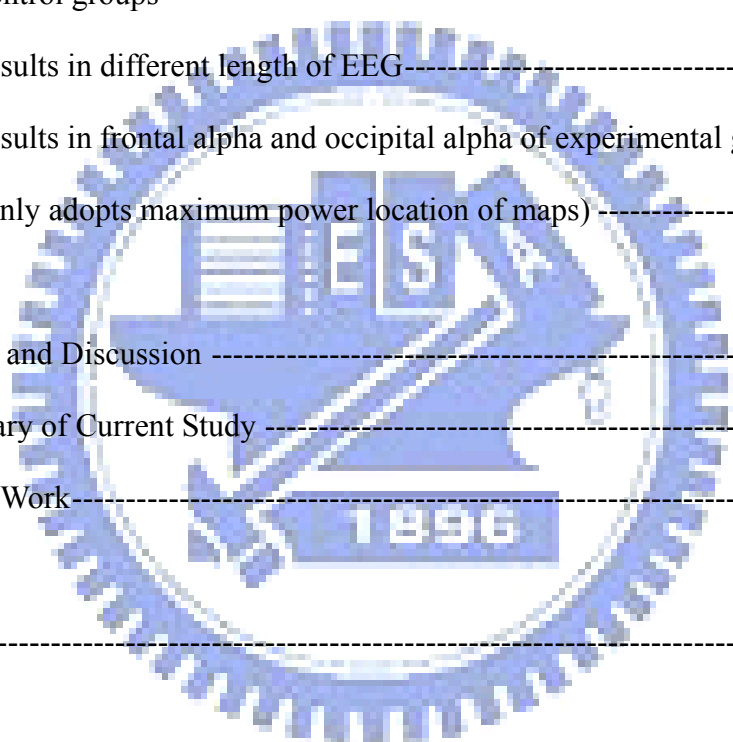
最後我也要感謝我的家人及女友對我唸書的全力支持，使我無後顧之憂，能夠全新專注在課業上並順利完成學業。



Contents

中文摘要	I
Abstract	II
誌謝	III
Contents	IV
List of Tables	VI
List of Figures	VII
1 Introduction	1
1.1 Motivation	2
1.2 Scope of thesis	3
2 Theories and Methods	4
2.1 Outline of the scheme	7
2.2 Alpha Wave Detection	9
2.3 Mahalanobis Fuzzy C-Means (MFCM)	10
2.3.1 Mahalanobis Distance	10
2.3.2 Mahalanobis Fuzzy C-Means Algorithm	13
2.3.3 The number of clusters	16
2.4 Brain Spatial Microstates	17
2.4.1 Global Field Power (GFP)	19
2.4.2 Segmentation Method	21
2.4.3 Selection of the Window of Extreme LAP Site	23
2.5 Experimental Protocol	24

3 Experimental Results -----	27
3.1 Results of Brain-Mapping Classification -----	27
3.1.1 Control Subjects -----	28
3.1.2 Experimental Subjects-----	33
3.2 Results of Microstate Analysis -----	37
3.2.1 Frontal-alpha and occipital-alpha microstate in experimental group-----	37
3.2.2 Comparison of occipital-alpha microstates in experimental and control groups -----	39
3.2.3 Results in different length of EEG-----	41
3.2.4 Results in frontal alpha and occipital alpha of experimental group (only adopts maximum power location of maps) -----	42
4 Conclusion and Discussion -----	46
4.1 Summary of Current Study -----	46
4.2 Future Work-----	47
References-----	48
Appendixes-----	52
A.1 Discrete Wavelet Transform -----	52
A.2 Mahalanobis Distance -----	56



List of Tables

2-1 Parameters and variables used in Mahalanobis FCM-----	14
2-2 Results of microstate analysis with different thresholds -----	24
2-3 Control subjects -----	25
2-4 Experiment subjects-----	26
3-1 Correlations between clusters-----	32
3-2 Distance between cluster centers -----	32
3-3 Number of each cluster and standard deviation of cluster members-----	32
3-4 Correlations between clusters-----	36
3-5 Distance between cluster centers-----	36
3-6 Number of each cluster and standard deviation of cluster members-----	36
3-7 Frontal-alpha (FA) and occipital alpha (OA) microstate analysis for experimental subjects (4-second epoch)-----	38
3-8 Microstate analysis of 4-second occipital alpha mappings for the experiment and control subjects-----	40
3-9 The microstate analysis results of 4-seconds EEG with the experiment subjects of frontal alpha (FA) and occipital alpha (OA) -----	42
3-10 The microstate analysis results of 4-seconds EEG with the experiment subjects of frontal alpha (FA) and occipital alpha (OA) with only maximum power adopted -----	44
3-11 The microstate analysis results of 4-seconds EEG with the experiment subjects of mediation (MD) and control subjects of relaxation (Relax) with only maximum power adopted -----	45

List of Figures

2-1 Electrode locations of the 30-channel recording montage-----	5
2-2 Flowchart of the entire scheme-----	8
2-3 Alpha detection: the session with $\rho \geq 50\%$ is defined as alpha dominated-----	9
2-4 The distances to the center of the data, (a) with the circles representing the equal EDs, (b) with the ellipses representing the equal MDs.-----	12
2-5 The GFP of 1 second EEG epoch-----	20
2-6 Experimental protocol-----	24
3-1 Results of interpretation and classification of EEG brain mappings for a control subject in the pre-session background recording (before main session of relaxation) --	29
3-2 Classification result of one control subject in the main-session recording -----	30
3-3 Classification result of one control subject in the post-session recording -----	31
3-4 Results of interpretation and classification of EEG brain mappings for an experimental subject in the pre-session background recording (before main session of meditation) -----	33
3-5 Classification result of one experimental subject in the main-session (Zen meditation) recording -----	34
3-6 Classification result of an experimental subject in the post-session recording (after main session of mediation).-----	35
3-7 Average duration of brain microstate segments(frontal alpha and occipital alpha)-----	38
3-8 Dipolar vector model for alpha brain microstate with the filed minimum and maximum represented by circle and black dot, respectively-----	39
3-9 Average duration of brain microstate segments(meditation and relaxation) -----	40
3-10 Dipolar vector model for alpha brain microstate with the filed minimum and maximum represented by circle and black dot, respectively.-----	41

3-11 Dipoles appear in one minute follow by the time -----	43
3-12 The representative maximum pole locations with the experimental subjects of frontal alpha (FA) and occipital alpha (OA) -----	44
3-13 The representative maximum pole locations between experimental subjects in mediation (MD) and control subjects in relaxation (Ralax)-----	45
A-1 Discrete Wavelet Decomposition-----	55
A-2 Discrete Wavelet Reconstruction-----	55
A-3 Extraction the alpha wave by the Wavelet Decomposition -----	56



Chapter 1 Introduction

Since Electroencephalography (EEG) was firstly recorded in 1927, the EEG signals have been intensively studied in clinical applications and medical science. Nowadays, EEG becomes an important clinical tool for diagnosing and monitoring the nervous system regarding normal or pathological conditions. In the field of EEG study, the spatial or topographical features provide an access to the detection of focal EEG phenomena that have a relationship to focal pathology [1], [2]. The spatial distribution of EEG features (to be called the “EEG mapping” or the “brain mapping”) over the scalp surface is thus of great importance. In clinical applications, its graphical display is an easy and straightforward aid to visual inspection of focal activities. A number of methods and techniques have been used for constructing the EEG mapping [16-22]. According to our study on Zen-meditation EEG during the past ten years, a number of EEG characteristics have been found to be evidently linked to the Zen-meditation practice. We have reported our findings on frontal alpha activity and beta-dominated phenomena, mainly from the temporal and spectral aspects. In this study, we particularly focused on EEG spatial properties during meditation.

In this chapter, we begin with the introduction of EEG researches in recent years and the

background of this study.

1.1 Motivation

Studies of meditation EEG have attracted a large number of researchers in life science and medicine since a half century ago. The EEG is normally composed of the following rhythmic components: δ -wave (0~4Hz), θ -wave (4~8Hz), α -wave (8~13Hz), β -wave (13~30Hz), and γ (30~70Hz). Researches during the past several decades have disclosed the phenomenon that particular EEG patterns correlated closely with some physiological, mental, or emotional states. For instance, occipital α -wave becomes dominant during the eye-closed relaxation. Significant and numerous achievements have been reported on EEG rhythmic and EEG spatial characteristics applied to brain abnormalities and such pathological case study as epilepsy [3-5] and Alzheimer's disease [6]. Accordingly, EEG has become a feasible tool for diagnosing neural disorder diseases.

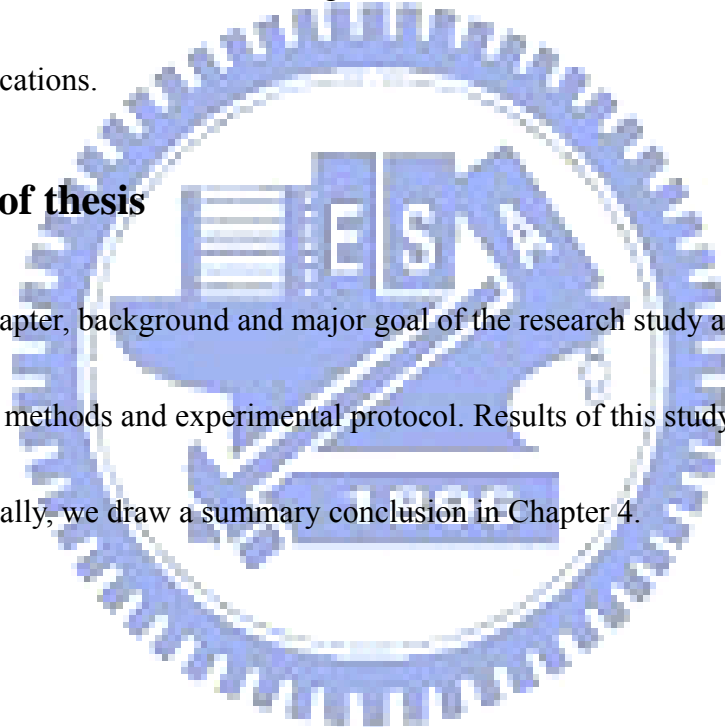
In the past two decades, scientists and medical experts have been getting more and more interested in meditation phenomena due to its benefits to human health[7-11]. A large variety of scientific approaches have been applied to meditation study. Since meditation process involves different states of consciousness, EEG thus became the focus of attention of

researchers. This thesis mainly reports the results of investigating the brain spatial microstates of α -wave for subjects practicing Zen meditation.

Most researches of brain spatial topography analyzed long-term EEG signal, but in some case of pathology, the phenomenon is transient or transitional. As epilepsy is a disease and can be detected by the momentary unusual EEG signal, and it is hard to find in long-term EEG analysis. So we used microstate algorithm for detection of transient brain state and hope for more applications.

1.2 Scope of thesis

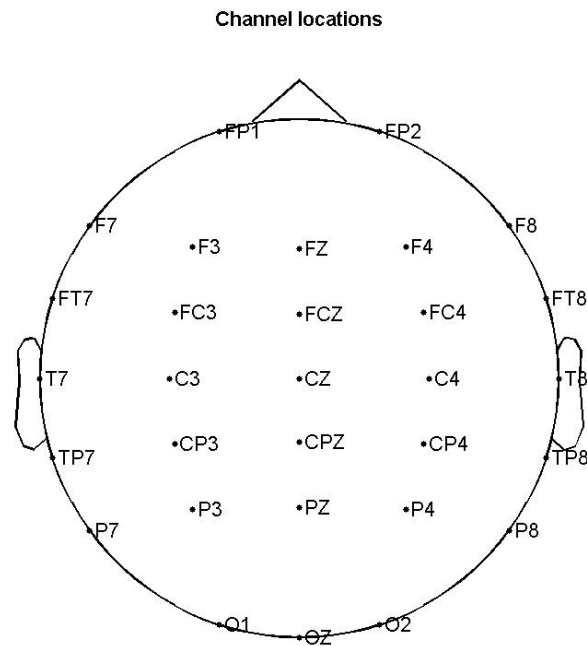
In this chapter, background and major goal of the research study are presented. Chapter 2 introduces the methods and experimental protocol. Results of this study are reported in Chapter 3. Finally, we draw a summary conclusion in Chapter 4.



Chapter 2 Theories and Methods

EEG (Electroencephalography) is the neurophysiologic measurement of the electrical activity of the brain by recording from electrodes placed on the scalp (non-invasive recording) or, in special cases, subdurally or in the cerebral cortex (invasive recording). The resulting traces are known as an electroencephalogram (EEG) and represent a summation of post-synaptic potentials from a large number of neurons. These are sometimes called brainwaves, though this use is discouraged, because the brain was not known to broadcast electrical waves. The EEG offers a medium for the brain function test, but in clinical use it is a "gross correlate of brain activity". We actually do not measure the electrical currents, but rather the potential differences between different parts of the brain

EEG applications in clinic have become more and more favorable because of its advantages of economy, safety, and convenience. EEG can be used for detecting apoplexy, epilepsy, cephalitis, etc. EEG studies have also been employed in patients who are deeply unconscious, to distinguish between brain death and possible reversible conditions. And it is also used to investigate other conditions that may affect brain function such as strokes, brain injuries, liver and kidney disease and dementia. In this study, we adopted 30-channel recording montage as shown in Figure 2.1.



30 of 30 electrode locations shown

Click on electrodes to toggle name/number

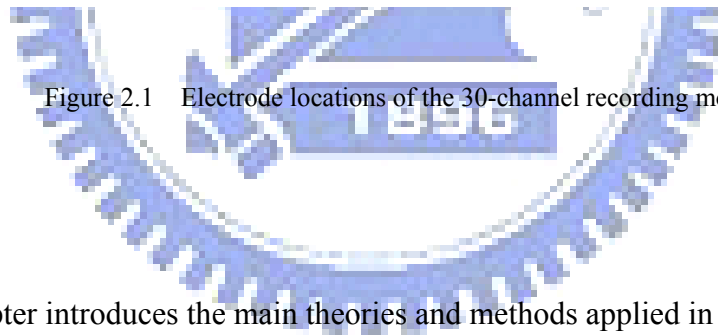


Figure 2.1 Electrode locations of the 30-channel recording montage.

This chapter introduces the main theories and methods applied in this study, including the wavelet transform, Mahalanobis distance (MD), fuzzy c-means, and the spatial-microstate analysis of the brain. The method for feature classification and clustering was named as Mahalanobis fuzzy c-means (MFCM) because we adopted the Mahalanobis distance in the fuzzy c-means algorithm.

This study was aimed to analyze the brain microstates for two groups of subjects:

Zen-meditation practitioners and normal, healthy persons within the same age group. The meditation duration lasted for almost 50 minutes. We extracted four-second segments for brain microstates analysis. How to select appropriate EEG segments, hence, became important. Our previous study demonstrated that frontal alpha was highly correlated with meditation state, differing from the occipital alpha often observed in normal subjects during eye-closed relaxation. Therefore, we focused on the analysis of the frontal-alpha brain microstates. The first task thus was to identify the occurrence of frontal-alpha activities. Hence we developed the pattern recognition technique to cluster the alpha activities into frontal-, parietal-, and occipital-alpha segments. And we analyzed the frontal and occipital alpha in meditation and the others (parietal alpha, occipital alpha) in relax by brain microstate.

The concept of MD includes the correlations of the data. We thus identified patterns of similarity based on this characteristic. In the study, brain spatial distributions were clustered by the approach of unsupervised pattern recognition. The aim was to group similar objects together. As a measure of similarity, the MD can be used to link similar populations together by computing the MD between population means (centroids). In combination with FCM, the MD replaced the Euclidean distance in the membership value function. Clustering scheme applying the fuzzy concept together with data correlation could achieve better efficiency. Results of clustering were then investigated by brain microstate analysis.

2.1 Outline of the scheme

The entire scheme applied in this study is illustrated in Figure 2.1. This block diagram describes the whole scheme correlating different theories and methods to accomplish our aim of characterizing the multi-channel EEG spatial behaviors. Following this flowchart, details of theories and methods will be introduced. To quantify alpha power, we applied wavelet analysis to 2-second windowed segments. Based on the block diagram in Figure 2.2, we then present the detailed concept and mathematics of each method in the following sections.

Firstly, EEG signals were pre-filtered by a band-pass filter with pass band 0.5 – 50 Hz. In the next step, wavelet analysis was applied to each 2-second EEG epoch to decompose raw EEG into characteristic rhythmic patterns. The epoch was identified to be alpha-dominated if the alpha power was at least 50% the total EEG power.

In MFCM (Mahalanobis Fuzzy C-means) clustering, we must find the initial cluster centers first. This study applied FCM for the determination of the initial centers. Difference between MFCM and FCM is that the correlation of data is adopted in MFCM's computation, and distance computation is related to the distribution of data. In some case of clusters that cannot be line-separated, but it could be work in MFCM. In microstate analysis, wavelet transform was applied to 131ms-windowed EEG that approximately enclosed the longest alpha-wave epoch. Because of we went to analysis the mini-second's brain state, so the

window would not too bigger and not too to extract the alpha-power.

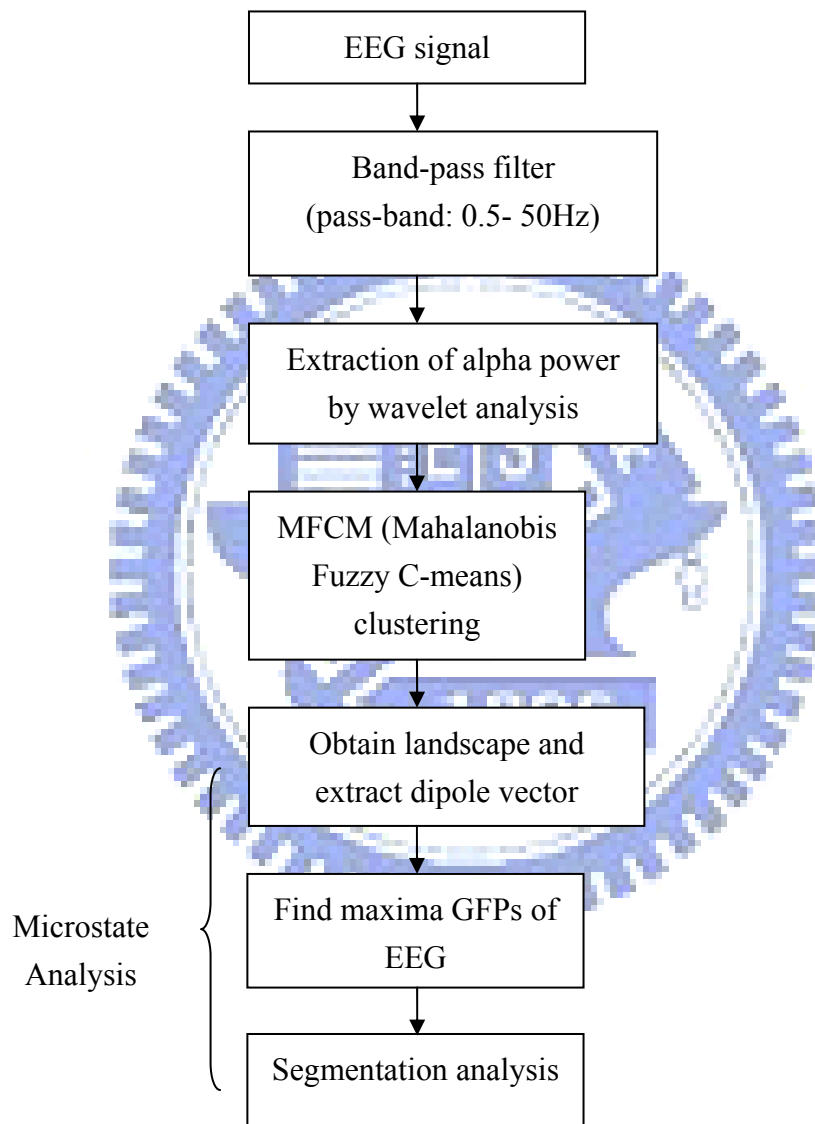


Figure 2.2 Flowchart of the entire scheme.

2.2 Alpha Wave Detection

For researching the effects of the alpha-wave, it is important to make sure that a trail of EEG is alpha dominate. We use wavelet transform to extract the wavelet coefficients of α , β , γ , δ , θ waves, and reconstructed them to calculate the α , β , γ , δ , θ power. Eq. (A.12), defines ρ as the percentage of α power to the total power. If $\rho \geq 50\%$ we call the EEG is alpha dominate.

$$\rho = \frac{P_{\alpha}}{P_{\alpha} + P_{\beta} + P_{\gamma} + P_{\delta} + P_{\theta}} \times 100\% \quad (2.1)$$

The figure 2.3 is a 5 seconds EEG signal, and we computed the ρ value in every one second. It is obviously that the signal is alpha dominate when $\rho \geq 50\%$, and when $\rho < 50\%$ the signal does not appears alpha-wave. It is easy to see that the method could detect alpha successfully. Because of the EEG signal have 30 channels, so we defined that if anyone channel is detected as alpha dominate, we can call this signal is alpha dominate.

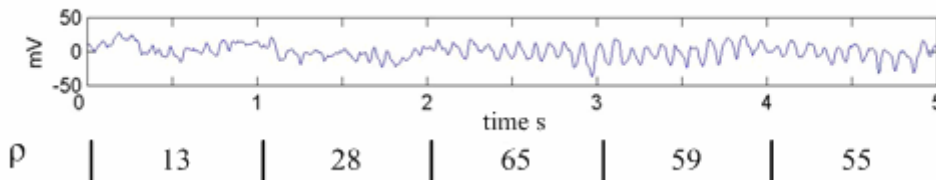


Figure 2.3 Alpha detection: the session with $\rho \geq 50\%$ is defined as alpha dominated.

2.3 Mahalanobis Fuzzy C-Means (MFCM)

Techniques based on the measurement of distances between quantitative features or attributes commonly apply such distance measures like Euclidean distance (ED) and Mahalanobis distance (MD). Both distances can be calculated either in the original variable space or in the principal component (PC) space. The ED is easy to compute and interpret, yet, this is not the case for the MD. Nevertheless, MD provides better results of feature clustering because it measures the correlations between variables[14,15]. In a sense, MD can be used to determine the degree of similarity of an unknown variable to the known one. It differs from Euclidean distance in that it takes into account the correlations of the data and is scale-invariant, that is, independent of the scale of measurements.

Fuzzy c-means (FCM) is a fuzzy classifier based on the cluster means. Instead of reaching a crispy decision like “0/1”, “true/false”, or “yes/no”, *fuzzy* allows the degree of truth of a statement ranging between 0 and 1. It is more suitable and feasible for classification and analysis of most empirical biomedical data. In this study, we employed MD distance measurement in the membership value of FCM and compared the difference of classification results with or without correlation computation.

2.3.1 Mahalanobis Distance

The correlation is calculated from the inverse of the variance-covariance matrix of the data. However, the computation of variance-covariance matrix could cause problems. When the empirical data are measured over a large number of variables (for example, channels), they may contain a large amount of redundant or correlated information. The resulting variance-covariance matrix may become a singular or nearly singular matrix that can not be inverted.

In the case of object- i with 30 dimensional map $x_i = (\mu_{i1}, \mu_{i2}, \dots, \mu_{i30})$, the ED with regard to the center map can be calculated for each object. Assume totally N objects, ED for object- i is computed as

$$ED_i = \sqrt{(\mu_{i1} - \bar{\mu}_1)^2 + (\mu_{i2} - \bar{\mu}_2)^2 + \dots + (\mu_{i30} - \bar{\mu}_{30})^2} \quad \text{for } i = 1 \text{ to } N, \quad (2.2)$$

Where μ_{i1} to μ_{i30} are the variables of object- i , $\bar{\mu}_1$ and $\bar{\mu}_{30}$ are the means the variables of center objects.

To be able to compute the MD, first the variance-covariance matrix C_x is calculated:

$$C_x = \frac{1}{(N-1)}(X_c)^T(X_c), \quad (2.3)$$

where the X is the data matrix containing N objects in the rows, X_c is the data matrix

X subtracted by the variable means \bar{X} ; $X_c = (X - \bar{X})$. For the 30 dimensional map, X

can be defined as :

$$X = \left[\begin{array}{cccc} \mu_{1,1} & \mu_{1,2} & \cdots & \mu_{1,30} \\ \mu_{2,1} & \mu_{2,2} & & \mu_{2,30} \\ \vdots & & \ddots & \vdots \\ \mu_{N,1} & \mu_{N,2} & \cdots & \mu_{N,30} \end{array} \right] \left. \vphantom{\begin{array}{c} \\ \\ \\ \end{array}} \right\} N \text{ subjects.} \quad (2.4)$$

The MD for object- i x_i is then

$$MD_i = \sqrt{(x_i - \bar{x})C_x^{-1}(x_i - \bar{x})^T} \quad (2.5)$$

where \bar{x} is the center of the data.

Figure 2.4(a) plots the simulated data for two variables μ_1 and μ_2 together with the circles representing the equal EDs with regard to the center point. Figure 2.4(b) plots the simulated data for two variables μ_1 and μ_2 together with the ellipses representing the equal MDs with regard to the center point. This example illustrates the effect of taking into account the variance-covariance matrix of the data points.

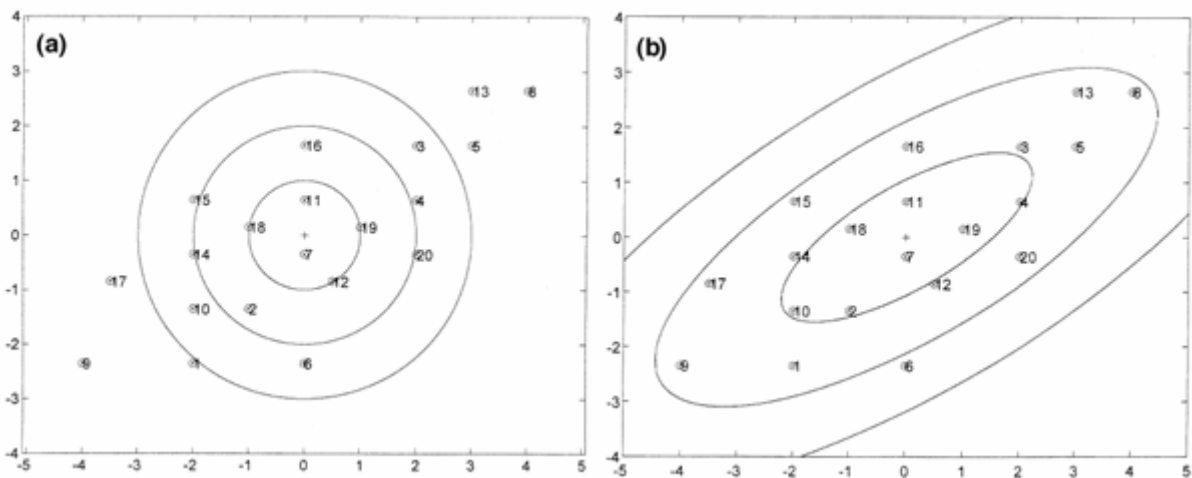
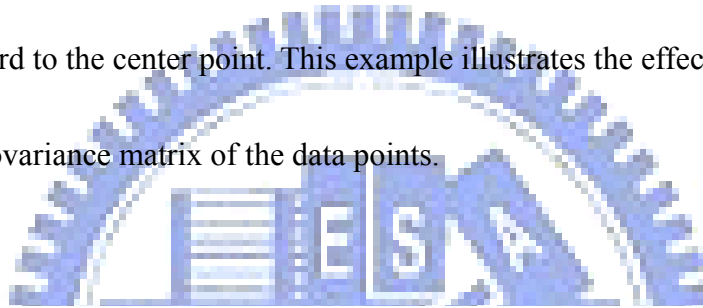


Figure 2.4 The distances to the center of the data, (a) with the circles representing the equal EDs, (b) with the ellipses representing the equal MDs.

2.3.2 Mahalanobis Fuzzy C-Means Algorithm

The fuzzy-based classification algorithm was improved by the scheme of c-means. By proper design of the membership function, we may improve the performance of classification.

FCM (Fuzzy c-means) is different from c-means. Method of c-means performs poorly when the data set is fuzzy.

In this study, we employed the Mahalanobis FCM algorithm. Mahalanobis FCM algorithm evaluates the MD instead of ED in the membership-function construction. To introduce Mahalanobis FCM, we firstly summarize the parameters and variables in Table 2.1.

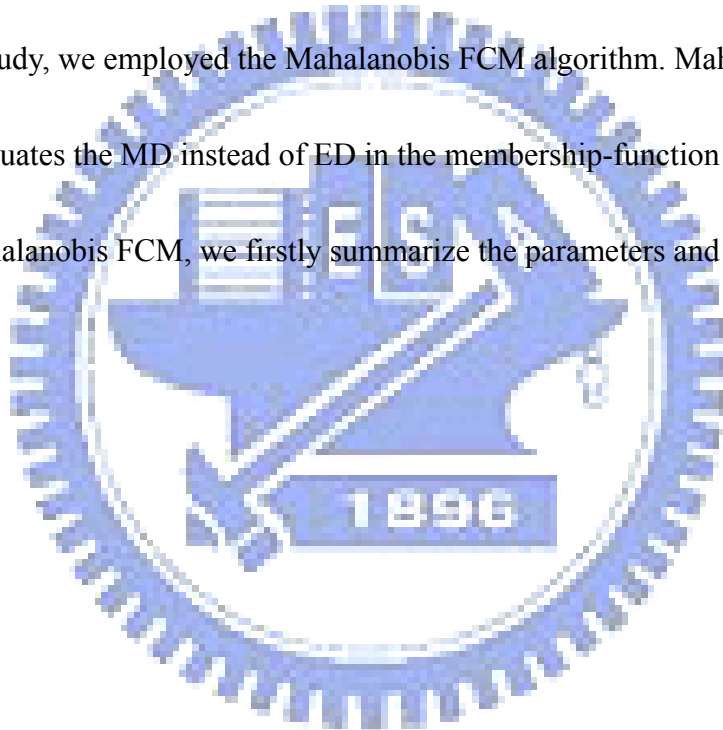


Table 2.1 Parameters and variables used in Mahalanobis FCM.

Parameters	
c	number of clusters
n_{ch}	the variable's degree
D	setting number of iterations
ε	allowed deviation
β	exponent weight
N	the number of objects
k	the computing iteration
$X = \{x_i 1 \leq i \leq N\}$	input data matrix, with every row is an object.
X_i	data matrix belonging to i^{th} class
$Y_0 = \{y_{i0}, 1 \leq i \leq c\}$	initial centers
Outputs	
$Y = \{y_i\}, 1 \leq i \leq c$	centers
$(\chi_{iy}), 1 \leq i \leq c, 1 \leq j \leq N$	membership value

The strategy of Mahalanobis FCM analysis is described below.

Step1 :

Initialization: $k = 0, y_{i,0} = y_{i0}, 1 \leq i \leq c$

Step2 :

Calculate the variance-covariance matrix and the MDs from data to centers

$$C_{i,k} = \frac{1}{(N-1)}(X_{i,k})^T(X_{i,k}), 1 \leq i \leq c \text{ and } 1 \leq j \leq N \quad (2.6)$$

$$d_{ij,k} = \sqrt{(x_j - y_{i,k})C_{i,k}^{-1}(x_j - y_{i,k})^T}, 1 \leq i \leq c \text{ and } 1 \leq j \leq N \quad (2.7)$$

Step3 :

Compute the membership value

$$\chi_{ij,k} = \left[\sum_{l=1}^c \left(\frac{d_{ij,k}}{d_{lj,k}} \right)^{\frac{2}{\beta-1}} \right]^{-1}, 1 \leq i \leq c \text{ and } 1 \leq j \leq N. \quad (2.8)$$

If $l = l_0$ and $d_{l_0j,k} = 0$, we let $\chi_{l_0j,k} = 1, \chi_{ij,k} = 0 (i \neq l_0)$

Step4 :

Compute the new centers by,

$$y_{i,k+1} = \frac{\sum_{j=1}^N \chi_{ij,k} x_j}{\sum_{j=1}^N \chi_{ij,k}} \quad (2.9)$$

Step5 :

$$\text{If } \left[\sum_{i=1}^c \|y_{i,k+1} - y_{i,k}\|^2 \right]^{\frac{1}{2}} < \epsilon,$$

let $y_i = y_{i,k+1}, 1 \leq i \leq c; \chi_{ij} = \chi_{ij,k}, 1 \leq i \leq c \text{ and } 1 \leq j \leq N.$

Terminate the iteration.

Step6 :

If $k = D$, terminate the iteration without attaining converged result.

If $k < D$, update the counter $k = k + 1$, repeat Steps 2 to 6.

Since the data have not been classified in the first run of iteration, X_i are not ready at the step 2. We thus need to initialize the values of X_i . Note that the resulted output may vary with the initial centers. Previous research showed that the initial centers significantly affected the output. In addition, we developed the scheme of estimating the initial centers by FCM and conducting feature clustering by Mahalanobis FCM.

2.3.3 The number of clusters

Beginning the clustering we should set the clustering numbers, and this number is decided by the correlation coefficients of the centers of clusters; when an correlation coefficients larger than θ that it indicates two cluster are similar, then the number will subtracted by one. So the initial number of clusters should be large. And in the past of our group's researches, we decided the $\theta = 0.3$ as an suitable number, the cluster could be distinguished in this situation.

2.4 Brain Spatial Microstates

Researchers have disclosed changes of alpha power in each cerebral-cortex region under different states. These studies show that spontaneous alpha exhibits different distributions owing to the variation of alpha sources or the propagation ways. Most substantially, alpha distribution might be related to the states of alertness. In these studies, alpha power was calculated by short-time spectral analysis based on Fourier-transformation method within a specific time window. Notice that Fourier approach is restricted by the piecewise stationary property that requires a narrow window of analysis and the frequency resolution that desires a wide window. In general, the window width is in the range from 1 to 5 seconds. However, from the viewpoint of the microscopic neural activities, the message is transmitted on the time scale of mini-second. The traditional FFT method is restricted to the window length and is difficult to explore the cerebral microstate.

In the research of Lehmann [16,17], he considered that the consistent neural activities would result in higher Global Field Power (GFP). The GFP is defined as the sum of the powers of all recoding channels at a specific sampling moment. The activity of each neuron could be considered as an electrical dipole vector including magnitude and direction. If each vector is uncorrelated with others, the activities would be canceled each other. In some

conditions, neurons are driven by the same source that leads to a large GFP. As larger GFP often infers better signal-to-noise ratio (SNR), the driven response can be more significant with less noise interference. The appearance of local maximal GFP's is thus an appropriate reference for choosing representative brain mappings (landscapes) to be utilized in the spatial microstate analysis. The sites of extremes (maximum and minimum) of a particular brain mapping compose a current dipole model generating the brain potential distribution recorded on the scalp.

We analyzed the brain microstates for a given time period 'segment'. A *segment* is a continuous time duration within which the electrode sites of maximal and minimal potential are almost immobile (staying in a small region). Alternatively speaking, dipole vectors within a *segment* are stationary in a sense. A spatial segmentation algorithm was developed to separate different segments of brain topographical activities. Each particular *segment* class contains brain mappings with two sites of extremes appearing most frequently at a given region. As a consequence, the method adopted in this thesis provides rather local and subtle temporal information which cannot be accessible based on conventional Fourier analysis.

Lehmann [16,17] used the raw EEG data (potentials on the recording sites) to extract the brain landscapes of interest. His method is not practicable for our aim on the analysis of alpha-rhythmic behaviors. We applied the alpha-power for the brain landscape for the microstate analyzing.

A number of approaches and methods have been developed to analyze the EEG signals in time, frequency, and spatial domains. A number of methods have been proposed to explore various EEG features, in either macroscopic or microscopic aspects. Each particular method calls for different lengths of EEG segments and different numbers of channels. In our study, we firstly performed feature clustering for 20 minutes EEG signals based on the spatial characteristics. Then those 4-second EEG epochs with particular topographic features were extracted for microstate analysis. We will demonstrate that, based on a short EEG epoch of only a few seconds, the microstates method provides a way of exploring the brain topographical behaviors under Zen meditation.

2.4.1 Global Field Power (GFP)

Global field power (GFP) at a given time instant represents the summation of EEG powers of all channels at that particular time t . A high GFP stands for a potential distribution with many peaks and troughs. According to [18], brain mappings with maximal GFP's normally have better SNR (signal-noise-ratio) performance. Hence, GFP provides a reference for us to select the appropriate time instants for microstates analysis. Assume a series A_k represents the data of channel- k . GFP is a function of time as shown below:

$$GFP(i) = \left[\frac{1}{n_{ch}} \sum_{k=1}^{n_{ch}} A_k^2(i) \right]^{1/2}, \quad (2.10)$$

Where i represents the time point of discrete time signal and n_{ch} is number of channel. In this thesis, the n_{ch} is defined as 30.

Figure 2.5 displays the GFP of a one-second EEG epoch. Apparently, GFP oscillates at a rhythm twice the EEG frequency due to the rectification effect.

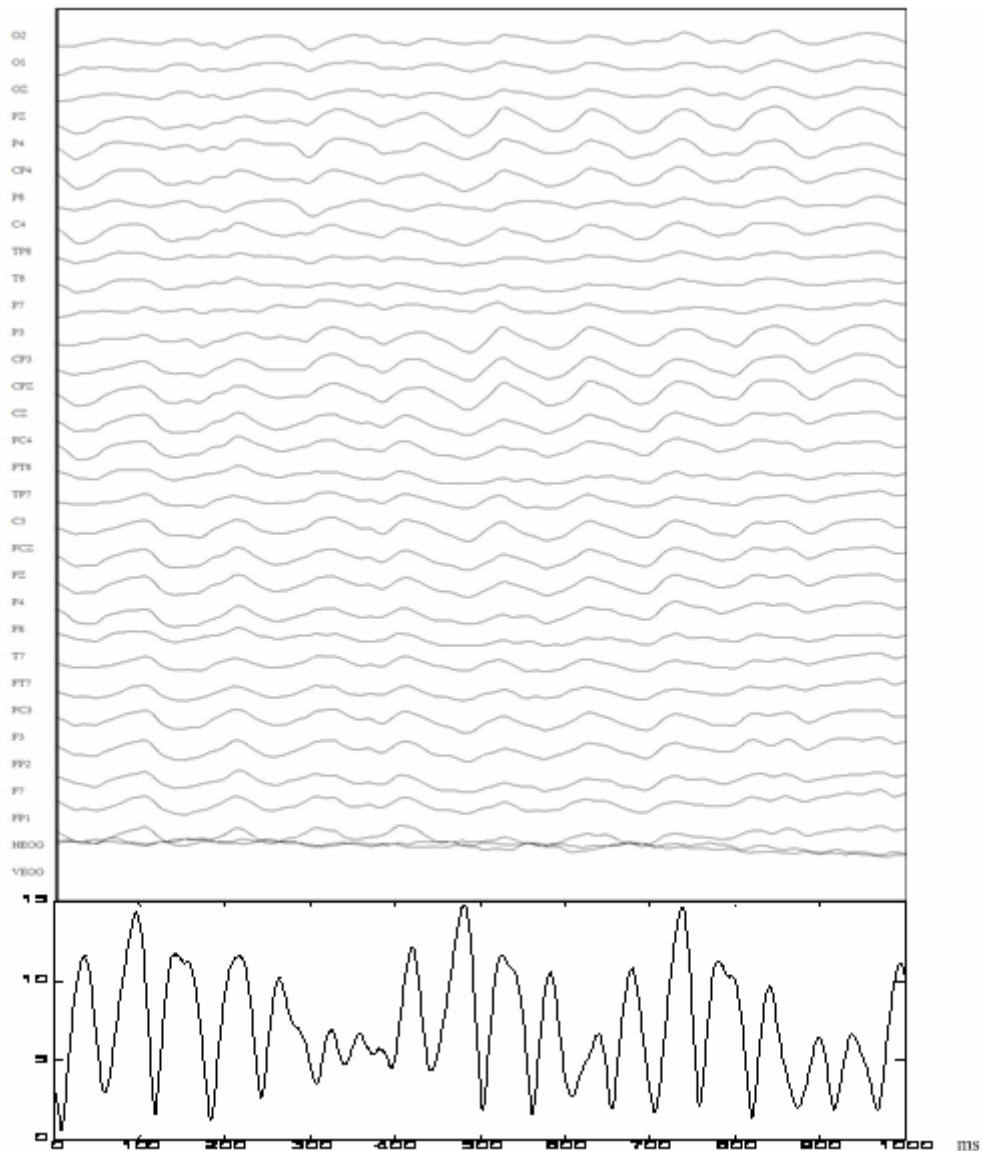
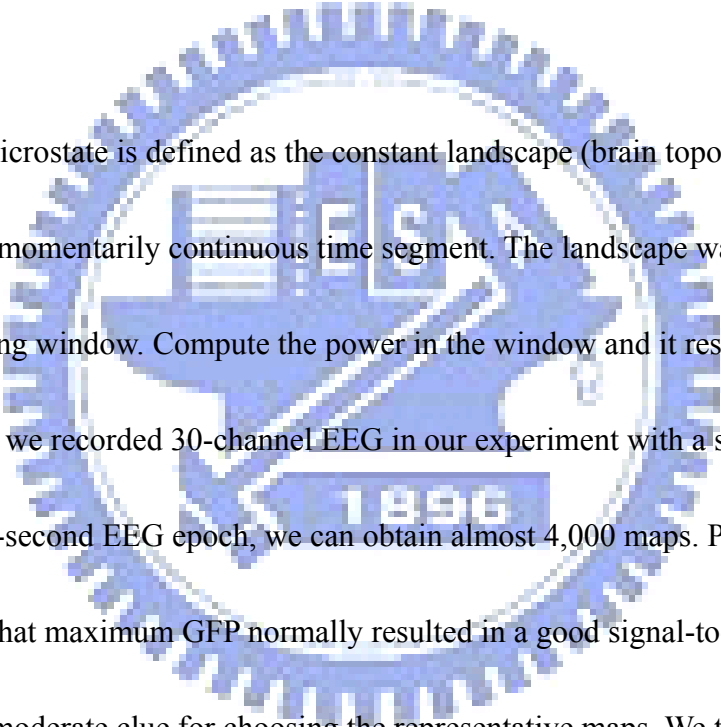


Figure 2.5 The GFP of 1 second EEG epoch.

Since alpha activity was our major focus, we applied wavelet decomposition to raw EEG to extract alpha-band (8-12Hz) patterns before the GFP evaluation. As a consequence, we could reduce the contamination from other rhythmic bands, for example, delta (0-4Hz), theta (4-8Hz), and beta (>20Hz). We then computed the GFP of alpha-dominated EEG.

2.4.2 Segmentation Method



A brain microstate is defined as the constant landscape (brain topographical mapping) that lasts for a momentarily continuous time segment. The landscape was obtained by a 131msec moving window. Compute the power in the window and it results a 30 dimensional map. Note that we recorded 30-channel EEG in our experiment with a sampling rate of 1,000 Hz. Within a 4-second EEG epoch, we can obtain almost 4,000 maps. Previous study [18] has demonstrated that maximum GFP normally resulted in a good signal-to-noise ratio. This is accordingly a moderate clue for choosing the representative maps. We thus focused on the locations of extremes (maximum and minimum power value) of brain mappings.

In our study, brain microstates are characterized by the current dipole vector pointing from the minimum to the maximum potential of the multichannel EEG mapping on the scalp. As a consequence, it becomes important to determine the appropriate locations (EEG channels) where extremes occur. Sometimes the extremes might be influenced by the noise. To deal with

the noise problem, we developed an approach for better extracting the extremes.

First, we employed the spherical-coordinate model of the EEG electrodes to compute the average distance D_n between Cz and each of the rest 29 electrode sites. We then computed the local average power (LAP) of brain potentials within the D_n -radius circle centered on each channel. From the set of 30 local average powers (LAP's), extremes (maximum and minimum) could be determined in a sense of better statistical significance. Finally, the centered electrode of maximal and minimal LAP forms the dipole vector of the brain microstate.

In order to obtain the data with an optimal SNR, only the maps at the peaks (local maxima) of GFP temporal sequence were selected for brain microstates analysis. These brain mappings were reduced to the locations of the extremes (maximum and minimum power value).

The so-called *segment* of a microstate begins with a particular brain potential map BPM_1 characterized by a given dipole vector, and continues as long as the succeeding maps at the GFP peaks come up with the same dipole vector. That is, minimal and maximal LAP locates at the same sites as those of the beginning dipole vector obtained from BPM_1 . The *segment* ends if the extreme LAP sites are out of range and continues if the sites are in the pre-defined range. The duration of a segment can be obtained straightforwardly. And the class of a segment is defined by the extreme LAP sites whose have the highest occurrence times.

In each group, we analyzed four parameters: a) number of maximum GFPs per seconds,

b) average duration of a segment, c) number of segments per second, and d) maximum duration of the segments.

2.4.3 Selection of the Window of Extreme LAP Site

In the microstates analysis, we need to designate a circular window for justifying whether the extreme LAPs belong to the same microstate. Table 2.2 lists the results of an experimental subject with frontal alpha obtained by different threshold (D_n : same as the D_n before, ie, average of 29 distances from Cz to others). The threshold is used as the radius of the circular window.

A larger threshold could cause the different microstates as the same state, and on the other hand, a smaller threshold could separate one microstate into several segments. Either a small or a large threshold may not reliably reflect the evolution of microstates, so we had to find a suitable range for this threshold. According to our experiment, the threshold in the range of $0.7D_n \sim 1.5D_n$ provides obviously different dipole vectors with the range of $0.5D_n$ and $2D_n$; while the locations of dipole vectors in range of $0.7D_n \sim 1.5D_n$ are about the same as the frontal alpha, so it represent that the efficacy of segmentation are quiet the same in this region. Hence the threshold in this range ($0.7D_n \sim 1.5D_n$) is feasible. This study adopted D_n as the threshold.

Table 2.2 Results of microstate analysis with different thresholds

Threshold	0.5 Dn	0.7Dn	Dn	1.5Dn	2Dn
Dipole strength (mv ²)	96.5	200	197	173	67
Dipole location	CPZ – O1	FCZ – P8	FCZ – P8	FZ – P8	O1 – TP8

2.5 Experimental Protocol

As illustrated in Figure 2.6, the entire recording experiment involved three sessions: pre-, mid-, and post-meditation session for experimental subjects who have been practicing Zen meditation, and pre-, mid-, and post-relaxation session for control subjects that are normal, healthy people within the same age range as the experimental subjects.

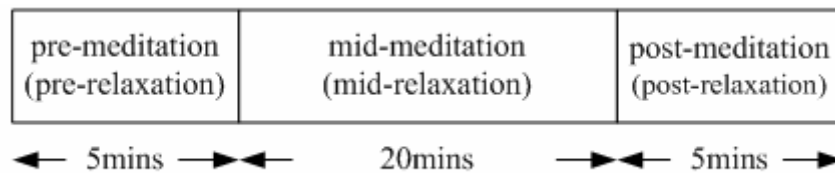


Figure 2.6 Experimental protocol.

In this study we selected eight healthy control subjects and eight healthy experiment subjects, and they were no medical or psychological disorders present. Tables 2.3 and 2.4 display the background of control subjects and experimental subjects, respectively

Table 2.3 Control subjects

Control subjects	Gender	Age
20040302	Male	24
20040315	Male	24
20040412	Male	23
20040414	Female	23
20040415	Female	23
20040422	Female	23
20040426	Female	22
20040428	Male	21

Table 2.4 Experiment subjects

Experiment subjects	Gender	Age	Meditation experience (years)
20040229	Female	29	7
20040306	Male	30	11
20040314	Female	21	1
20040318	Male	22	2
20040326	Male	28	8
20040520	Male	31	2
20040605	Male	34	7
20040711	Male	28	8



Chapter 3 Experimental Results

Chapter 3 discusses the experimental results of this research study. The content is organized according to two main tasks conducted in the study: 1) EEG spatial feature analysis and classification, and 2) brain microstate analysis, which are presented in Sections 3.1 and 3.2, respectively.

Inter-subject and intra-subject variations of EEG signals are inevitable and significant. Brain spatial microstate is undoubtedly time-dependent. Hence it is important to select the epoch of interest from the long EEG record. We used the spatial (brain-mapping) classification scheme to extract consecutive four-second epoch within the same class; and then analyzed the microstate of the epoch. This chapter presents the results of spatial classification and microstate analysis.

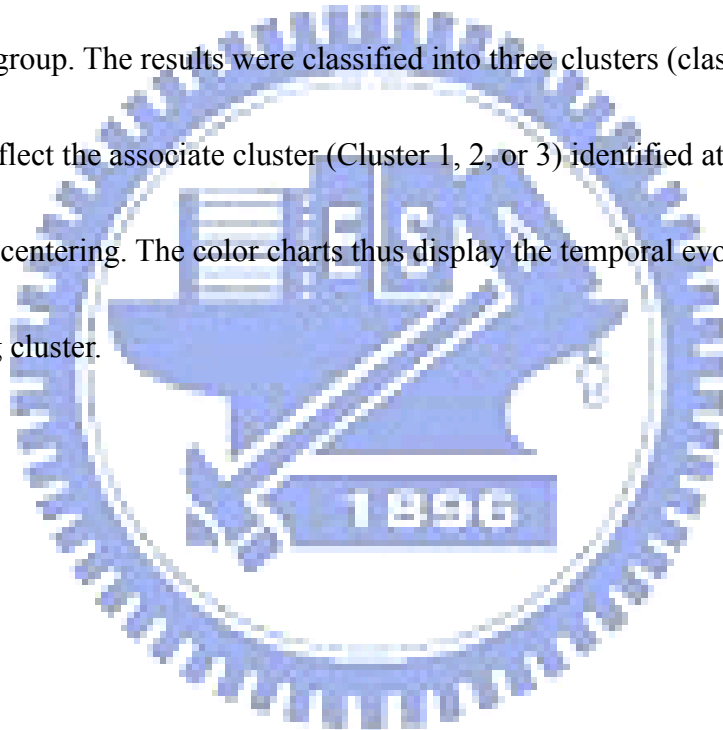
3.1 Results of Brain-Mapping Classification

In this section, we report the results of classifying brain topographical mappings by Mahalanobis FCM. In addition, results are compared between experimental and control group. As mentioned in 2.1, wavelet analysis was applied to each 2-second (pre-filtered by a band-pass filter) EEG epoch to decompose raw EEG into characteristic rhythmic patterns. The

epoch was identified to be alpha-dominated if the alpha power was at least 50% the total EEG power

3.1.1 Control Subjects

Figures 3.1-3.3 display the classification results of one representative subject (20040315) in the control group. The results were classified into three clusters (classes). Notice that the color charts reflect the associate cluster (Cluster 1, 2, or 3) identified at the time instant of the 2-sec window centering. The color-charts thus display the temporal evolution of brain-mapping cluster.



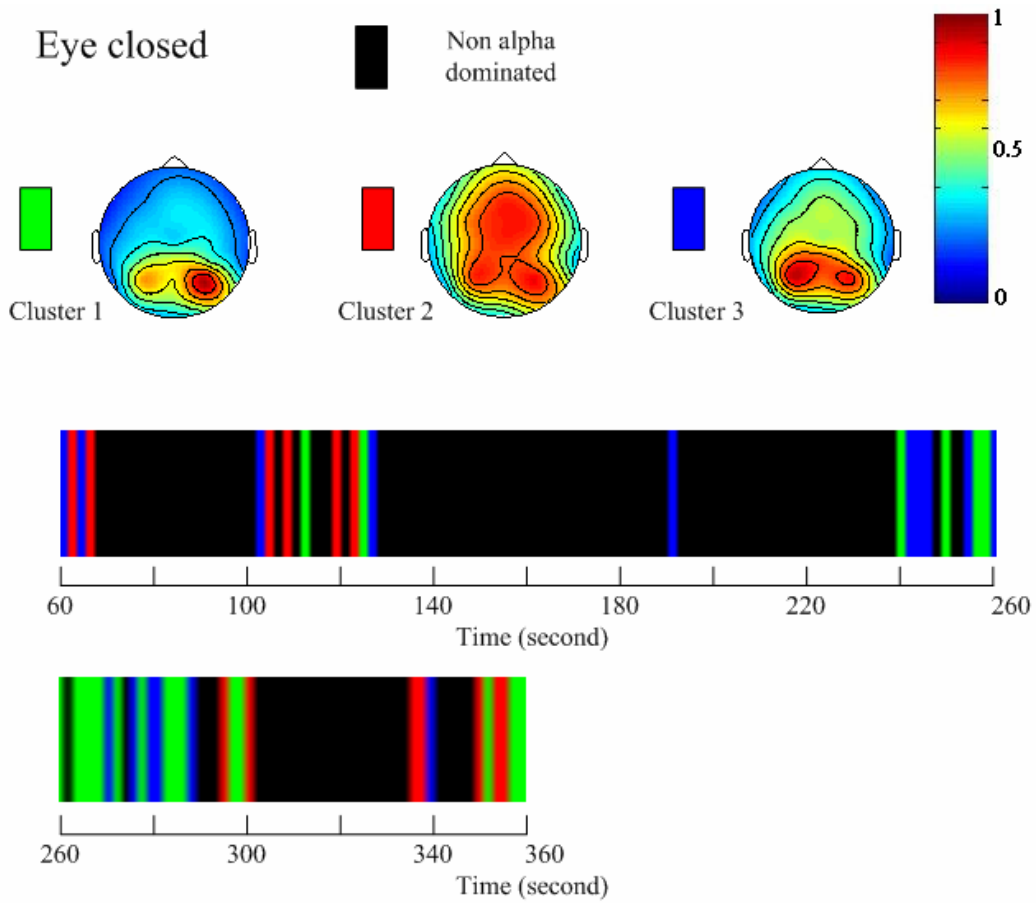


Figure 3.1 Results of interpretation and classification of EEG brain mappings for a control subject in the pre-session background recording (before main session of relaxation).

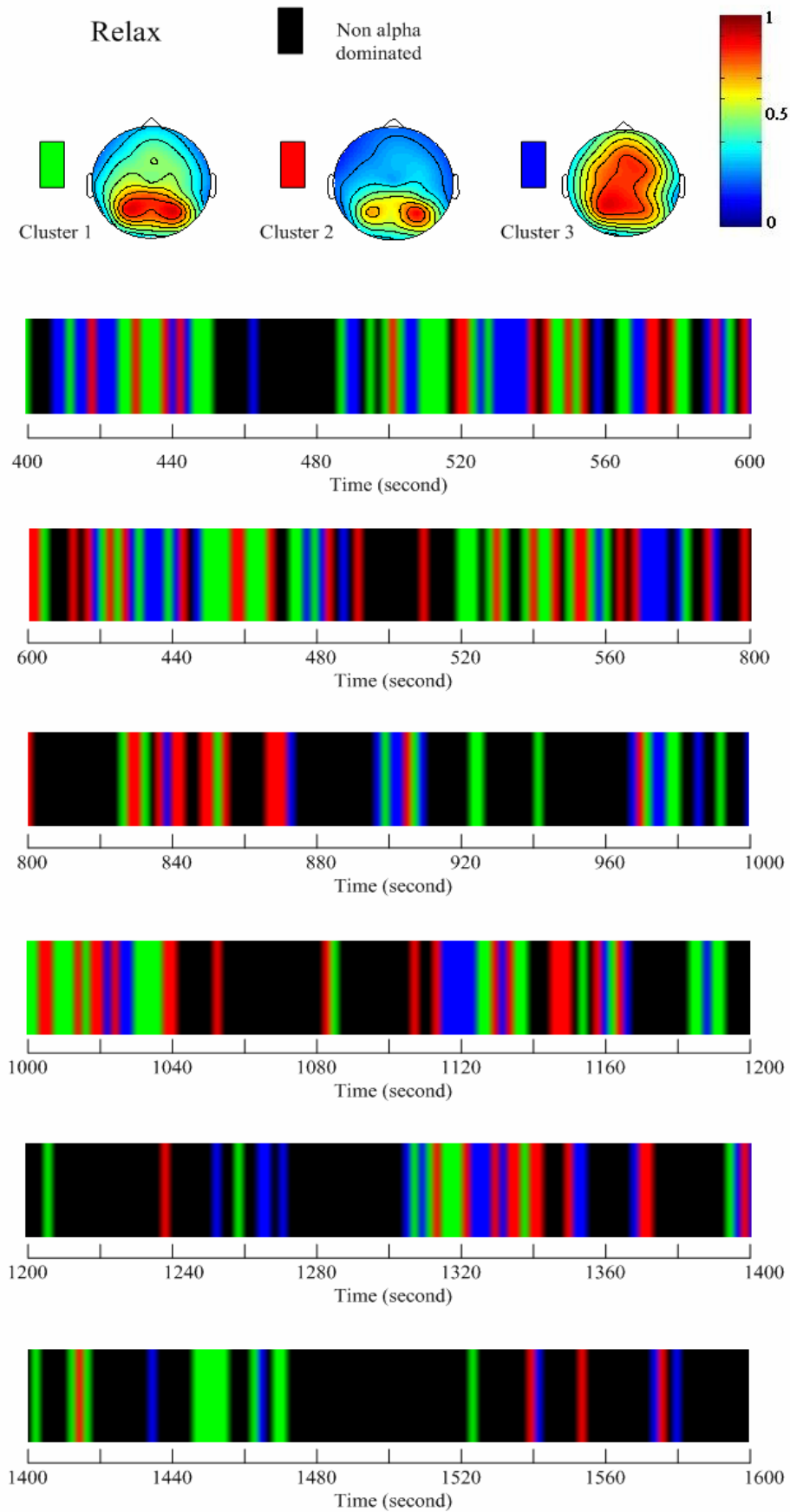


Figure 3.2 Classification result of one control subject in the main-session recording.

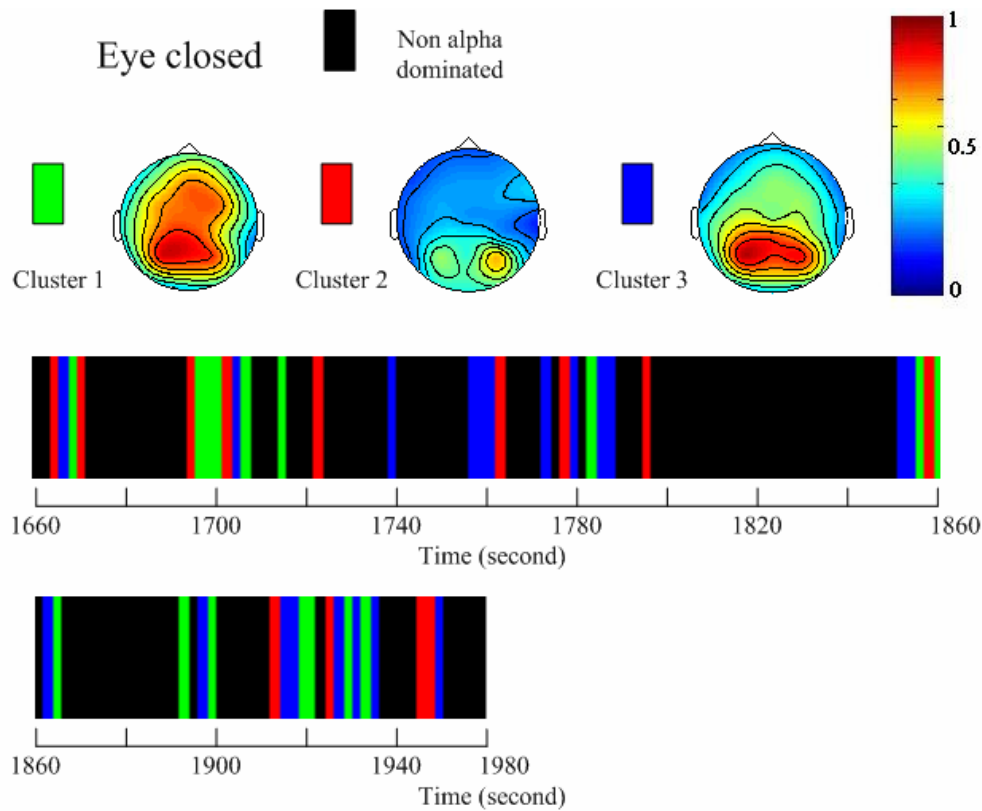


Figure 3.3 Classification result of one control subject in the post-session recording.

According to the results in Figures 3.1-3.3, all clusters derived contained no frontal-alpha activity for all the recording sessions. Very few control subjects had frontal alpha cluster. Table 3.1 shows the correlations between each pair of cluster centers. Table 3.2 lists the distance between each pair of cluster centers, while Table 3.3 lists the standard deviation of all members belonging to the same cluster. The inter-cluster distance were larger than the within-cluster standard deviation, justifying the effectiveness of this classification scheme.

Table 3.1 Correlations between clusters

Cluster\Cluster	1	2	3
1	1	-0.105	-0.585
2	-0.105	1	-0.745
3	-0.585	-0.745	1

Table 3.2 Distance between cluster centers

Cluster\Cluster	1	2	3
1		0.742	0.905
2	0.742		1.5773
3	0.905	1.5773	

Table 3.3 Number of each cluster and standard deviation of cluster members

Cluster	number	Standard deviation
1	109	0.550
2	87	0.675
3	86	0.646

3.1.2 Experimental Subjects

Figures 3.4-3.6 display the interpretation and classification results of an experimental subject (20040306). Three clusters were derived. Same as previous figures, the color bar charts display the temporal evolution of brain-mapping cluster.

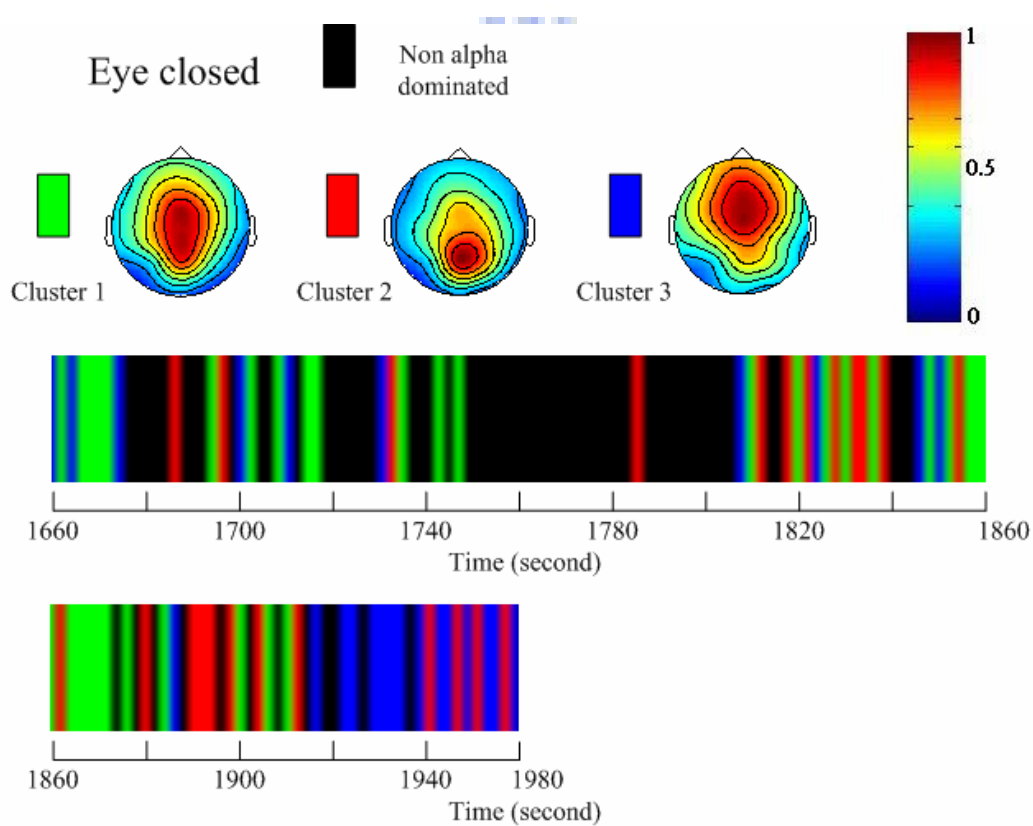


Figure 3.4 Results of interpretation and classification of EEG brain mappings for an experimental subject in the pre-session background recording (before main session of meditation).

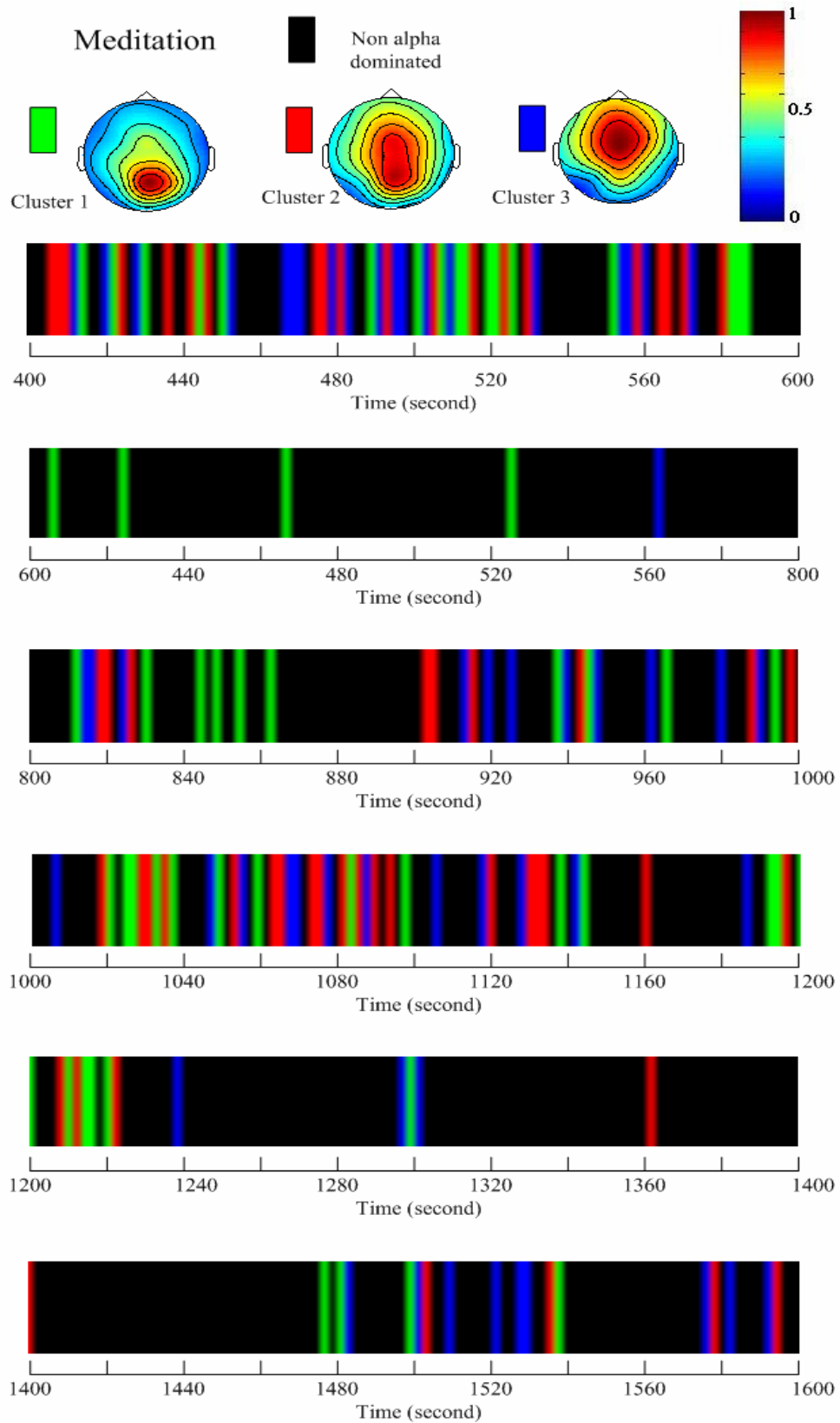


Figure 3.5 Classification result of one experimental subject in the main-session (Zen meditation) recording

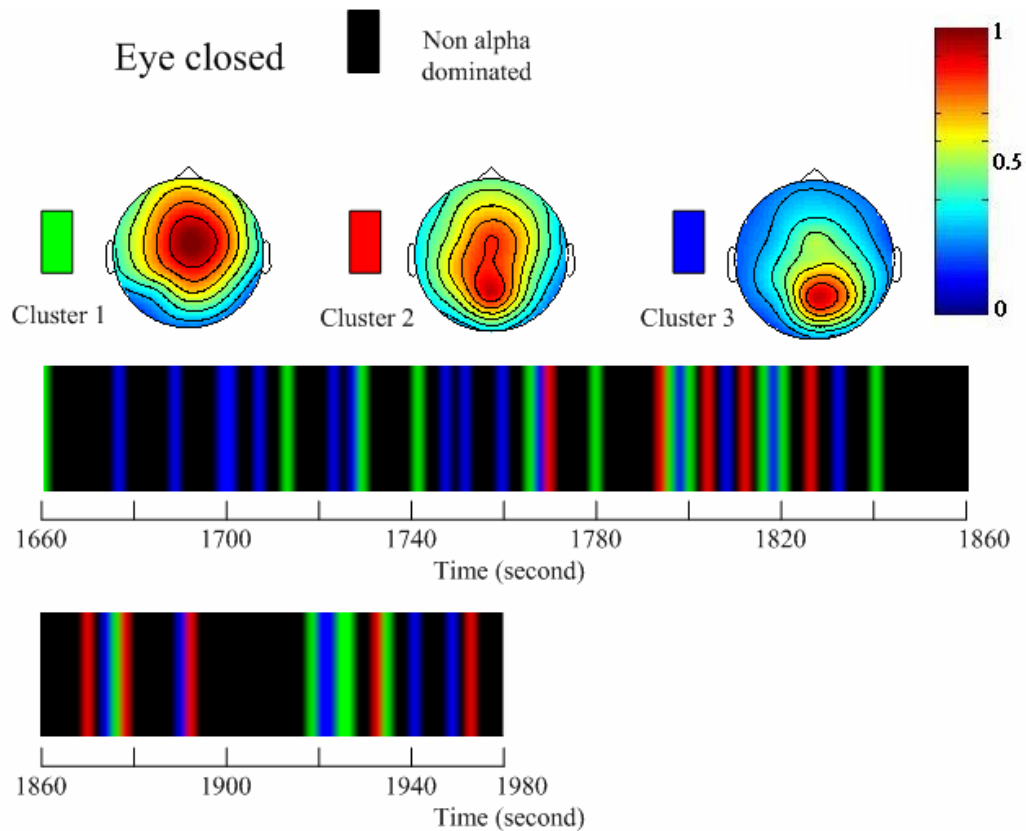


Figure 3.6 Classification result of an experimental subject in the post-session recording (after main session of mediation).

From Figures 3.4-3.6, alpha activities apparently moved toward the frontal regions for the meditation subject. In addition, frontal alpha increased in the meditation session that occupied approximately one-third record length of the main session. Table 3.4 shows the correlations between the three class centers, and the table 3.5 3.6 show the distance between centers and the standard deviation. The distances between centers are also larger than the standard deviation.

Table 3.4 Correlations between clusters

Cluster\Cluster	1	2	3
1	1	-0.620	-0.851
2	-0.620	1	0.116
3	-0.851	0.116	1

Table 3.5 Distance between cluster centers

Cluster\Cluster	1	2	3
1		0.938	1.390
2	0.938		0.624
3	1.390	0.624	

Table 3.6 Number of each cluster and standard deviation of cluster members

Cluster	number	Standard deviation
1	55	0.603
2	57	0.632
3	55	0.525

3.2 Results of Microstate Analysis

In the analysis of brain topographic (or, spatial) microstates, we focused on particular features extracted by classification in previous sub-section. For the experimental group with Zen- meditation experience, four-second frontal alpha and occipital alpha were selected. However, control subjects in this study appeared to have rare frontal-alpha activity. We accordingly only analyzed the four-second occipital alpha for the control group.

3.2.1 Frontal-alpha and occipital-alpha microstate in experimental group

According to the results in Table 3.7 and Figure 3.7, average duration of the alpha brain microstate demonstrates that frontal alpha exhibits a longer, continuous average duration of microstate. Figure 3.8 displays the results of dipolar-vector representation for modeling frontal-alpha (FA) and occipital-alpha (OA) microstates. One phenomenon to be further investigated is that, FA (OA) dipoles might emerge in the regions other than frontal (occipital) area.

Table 3.7 Frontal-alpha (FA) and occipital alpha (OA) microstate analysis for experimental subjects (4-second epoch).

Subject	1	2	3	4	5	6	7	8	Mean	S.D.
Number of maximum GFPs per second										
FA	25	26.8	28.5	22.8	23	25.8	28.3	20.8	25.1	2.8
OA	27.5	26.5	27.5	26	28.5	24.8	29.8	23.3	26.7	2.1
Average duration of an alpha brain microstate (in ms)										
FA	77.0	82.2	83.1	67.4	99.3	88.2	80.2	92.9	83.8	9.8
OA	63.9	88.7	64.5	70.0	77.5	70.2	58.0	79.3	71.5	9.9
Number of alpha brain microstates per second										
FA	7	6	6	6	6	7	7	5	6.3	0.7
OA	7	7	7	6	5	6	9	6	6.8	1.0
Maximum duration of an alpha brain microstate (in ms)										
FA	198	251	237	221	251	242	197	172	221	29
OA	187	182	202	245	278	187	167	163	201	40

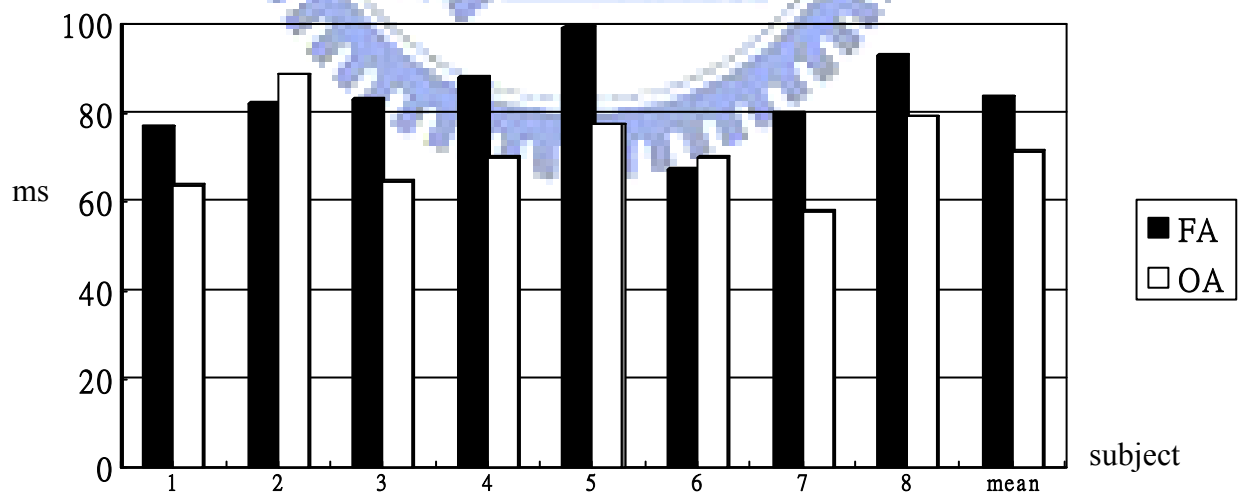


Figure 3.7 Average duration of brain microstate segments(frontal alpha and occipital alpha)

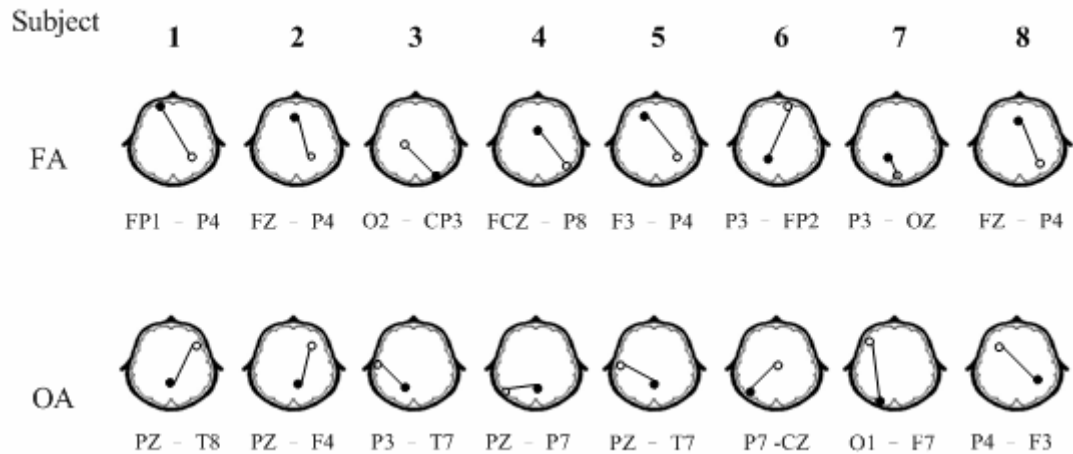


Figure 3.8 Dipolar vector model for alpha brain microstate with the filed minimum and maximum represented by circle and black dot, respectively.

3.2.2 Comparison of occipital-alpha microstates in experimental and control groups

The result of average duration of microstate for these two groups shows no obviously difference (meditation subjects: 71.5; relax subjects: 68.4). Although the control group's number of microstates is little larger, but its duration is less than experimental group. So we think there is no very difference between these two groups. The figure 3.10 shows the locations of the two extreme poles, because of the analyzing signal selection of these two group is occipital alpha, the most locations are match with the classification result.

Table 3.8 Microstate analysis of 4-second occipital alpha mappings for the experiment and control subjects.

Subject	1	2	3	4	5	6	7	8	Mean	S.D.
Number of maximum GFPs per second										
MD	28	27	28	26	29	25	30	23	26.7	1.9
Relax	22	25	26	27	24	27	25	27	25.3	1.7
Average duration of an alpha brain microstate (in ms)										
MD	63.9	88.7	64.5	70.0	77.5	70.2	58.0	79.3	71.5	9.9
Relax	73.8	75.8	63.7	63.4	69.3	69.6	51.5	79.8	68.4	8.8
Number of alpha brain microstates per second										
MD	7	7	7	7	5	6	9	6	6.6	1.0
Relax	6	6	7	8	6	7	7	5	6.3	0.8
Maximum duration of an alpha brain microstate (in ms)										
MD	187	182	202	245	278	187	167	163	201	40
Relax	241	161	188	234	202	247	171	197	205	32

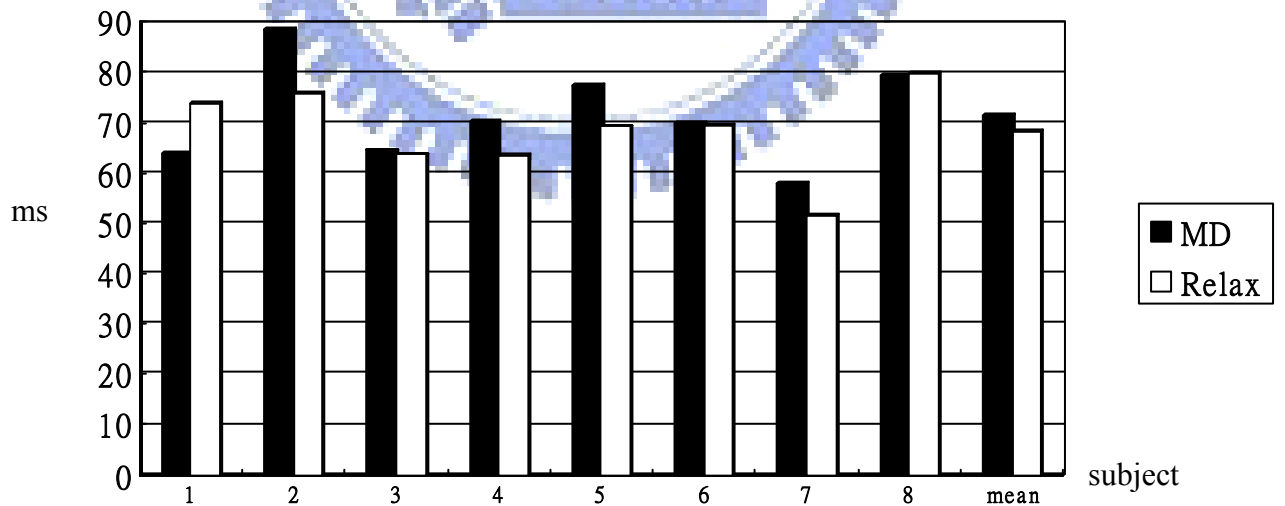


Figure 3.9 Average duration of brain microstate segments(mediation and relaxation)

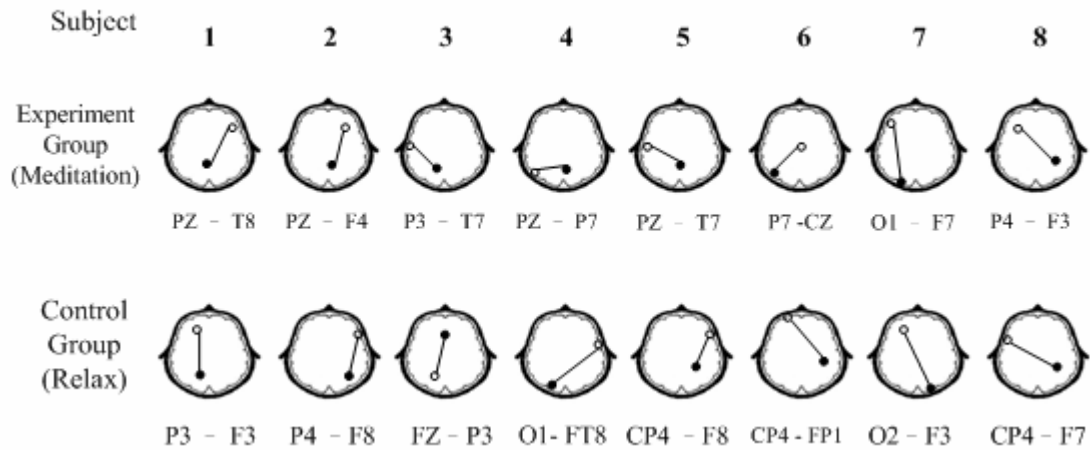


Figure 3.10 Dipolar vector model for alpha brain microstate with the filed minimum and maximum represented by circle and black dot, respectively.

3.2.3 Results in different length of EEG

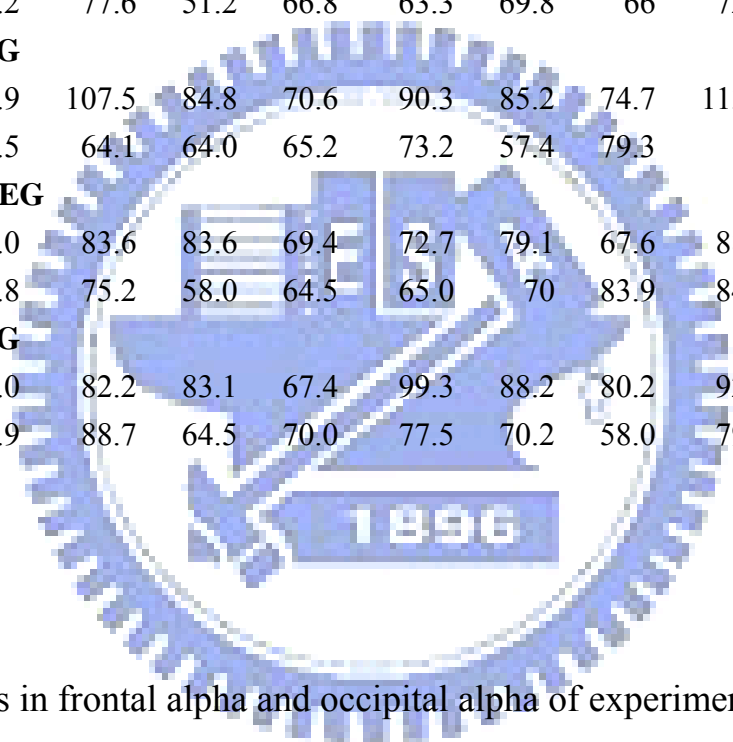
Since the research of microstates[18] used four seconds EEG for analysis, and the average duration of microstate are about 60~100 ms. So we interest that the analysis time can be reduced or not. The following table 3.9 shows the results of microstate analysis in different length of EEG signal (2, 2.5, 3, 3.5, and 4 seconds) in frontal alpha and occipital alpha of experimental group. The result shows the same thing that the average duration of microstate in frontal alpha is longer than in occipital alpha.

Table 3.9 The microstate analysis results of 4-seconds EEG with the experiment subjects of frontal alpha (FA)

and occipital alpha (OA)

Average duration of alpha brain microstate

Subject	1	2	3	4	5	6	7	8	Mean	S.D.
2 seconds EEG										
FA	62.6	86	67	80.1	90.7	92.8	77.3	70.5	78.4	11.1
OA	57.7	104.5	60.1	67.5	77.5	84.8	73.4	70.8	74.6	15.0
2.5 seconds EEG										
FA	73.2	89.3	75.7	89.3	115.8	89.2	68.7	118.9	90.0	18.7
OA	41.2	77.6	51.2	66.8	63.3	69.8	66	72.1	63.5	11.8
3 seconds EEG										
FA	68.9	107.5	84.8	70.6	90.3	85.2	74.7	113.5	86.9	16.4
OA	63.5	64.1	64.0	65.2	73.2	57.4	79.3	95	70.2	12.1
3.5 seconds EEG										
FA	67.0	83.6	83.6	69.4	72.7	79.1	67.6	88.7	76.5	8.4
OA	72.8	75.2	58.0	64.5	65.0	70	83.9	84.6	71.8	9.4
4 seconds EEG										
FA	77.0	82.2	83.1	67.4	99.3	88.2	80.2	92.8	83.8	9.8
OA	63.9	88.7	64.5	70.0	77.5	70.2	58.0	79.3	71.5	9.9



3.2.4 Results in frontal alpha and occipital alpha of experimental group (only adopts maximum power location of maps)

In 3.2.1~3.2.3, most of results of Average duration of an alpha brain microstate are less than 100 m-seconds, which is considered as a shorter duration of state. So we shown the dipoles(in maxima GFPs) in one minute (Fig 3.11). And we found that the location of minimum power changed frequently, the minimum power location is usually in the edge; but

the values of power in the edge locations are very close, so we think the frequently changed location of minimum power cause the results of duration of alpha brain microstate shorter. Hence following shows the microstate results which the segment only adopts the maximum power location.

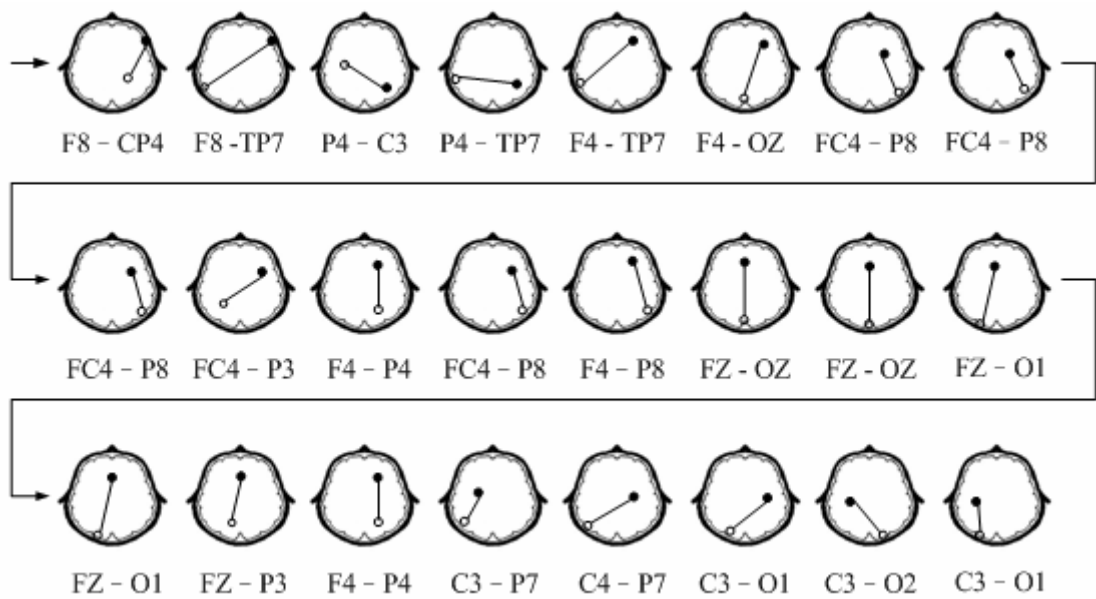


Figure 3.11 Dipoles appear in one minute follow by the time

Table 3.10 showed the results of experimental subjects of FA and OA, the average duration of an alpha brain microstate of FA is 208 m-sec that is longer than OA's, and the maximum microstate duration is 517 m-sec also longer than OA's. And table 3.11 showed the results between experimental subjects and control subjects (occipital alpha); the difference of results is not obviously. The figure 3.12 and figure 3.13 shows maximum poles locations, and it generally matches with the brain mappings.

Table 3.10 The microstate analysis results of 4-seconds EEG with the experiment subjects of frontal alpha (FA)

and occipital alpha (OA) with only maximum power adopted

Subject	1	2	3	4	5	6	7	8	Mean	S.D.
Number of maximum GFPs per second										
FA	25	27	23	25	24	25	27	22	25	1.7
OA	25	26	25	24	23	26	28	23	25	1.7
Average duration of an alpha brain microstate (in ms)										
FA	206	148	234	328	219	172	145	195	208	59
OA	168	115	197	226	167	199	142	193	175	35
Number of alpha brain microstates per second										
FA	4	5	3	3	3	6	3	4	4	1.1
OA	4	6	4	4	5	4	5	4	5	0.8
Maximum duration of an alpha brain microstate (in ms)										
FA	474	393	524	767	736	397	350	492	517	156
OA	451	318	597	576	348	550	394	580	477	113

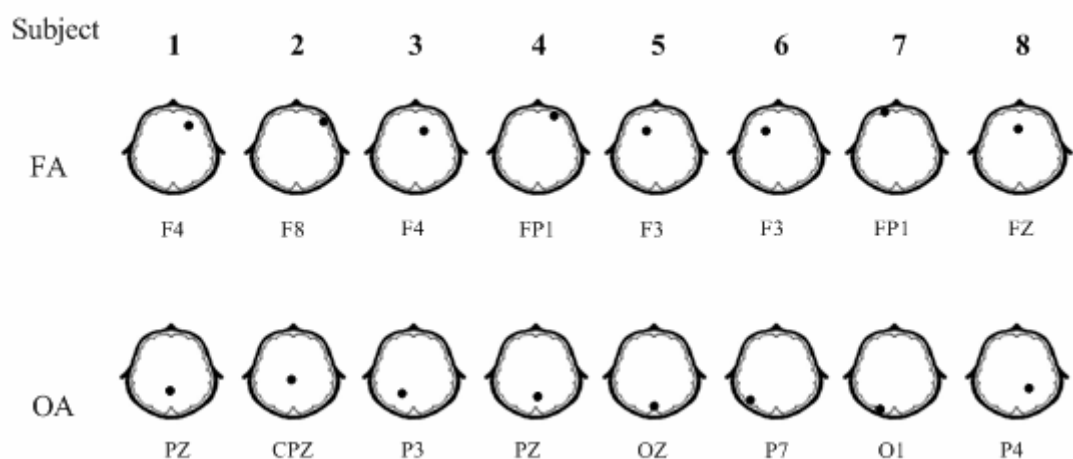


Figure 3.12 The representative maximum pole locations with the experimental subjects of frontal alpha (FA) and

occipital alpha (OA).

Table 3.11 The microstate analysis results of 4-seconds EEG with the experiment subjects of mediation (MD)

and control subjects of relaxation (Relax) with only maximum power adopted

Subject	1	2	3	4	5	6	7	8	Mean	S.D.
Number of maximum GFPs per second										
MD	25	26	25	24	23	26	28	23	25	1.7
Relax	26	26	24	25	25	27	26	27	26	1.1
Average duration of an alpha brain microstate (in ms)										
MD	168	115	197	226	167	199	142	193	175	35
Relax	193	126	165	234	152	215	129	138	169	41
Number of alpha brain microstates per second										
MD	4	6	4	4	5	4	5	4	5	0.8
Relax	5	5	5	4	4	4	5	6	5	0.7
Maximum duration of an alpha brain microstate (in ms)										
MD	451	318	597	576	348	550	394	580	477	113
Relax	497	249	388	455	502	475	511	379	432	89

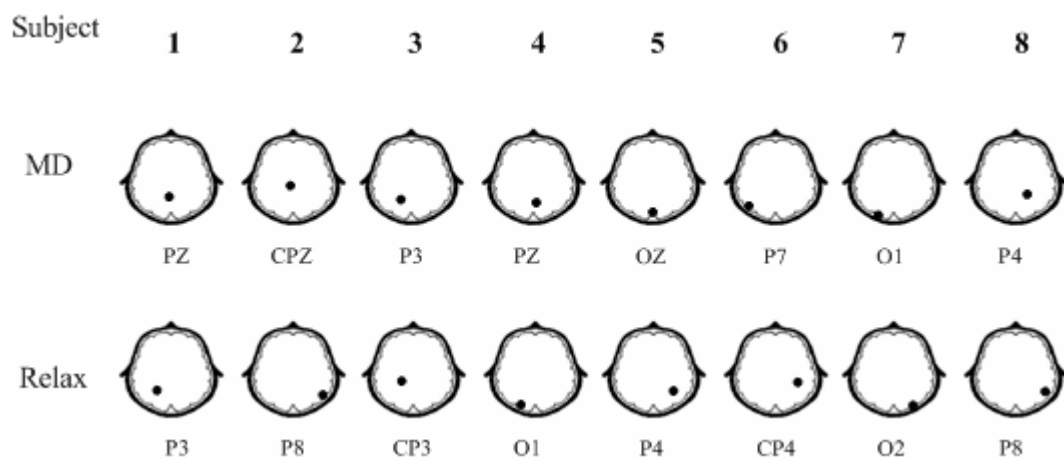
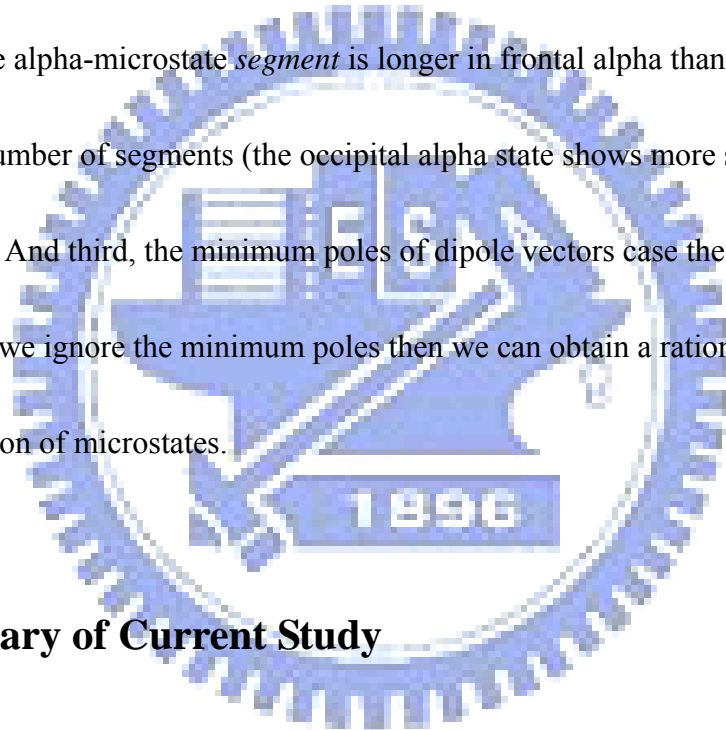


Figure 3.13 The representative maximum pole locations between experimental subjects in mediation (MD) and control subjects in relaxation (Relax).

Chapter 4 Conclusion and Discussion

In this thesis, we mainly proposed a novel approach for analyzing the spatial-temporal characteristics of various alpha rhythms down to the micro-second portrait, instead of long-time property. In our findings, experimental subjects apparently exhibited more frontal alpha than control subjects. Preliminary results are summarized as follows. Firstly, average duration of the alpha-microstate *segment* is longer in frontal alpha than in occipital alpha. Second, the number of segments (the occipital alpha state shows more segments than does frontal alpha). And third, the minimum poles of dipole vectors cause the average duration shorter, when we ignore the minimum poles then we can obtain a rational number of the average duration of microstates.



4.1 Summary of Current Study

In this thesis we provide a clustering method for the alpha brain maps classification and it performed efficiently. And the classification results are tend to separated into frontal, central and occipital, so that is useful to us choosing the alpha state characteristics for the microstate analysis. In the results of microstate analysis shows obviously difference of the frontal alpha group and occipital alpha group in mediation, the longer duration of microstate occurs with

frontal alpha than with occipital alpha. And some research shows that in meditation, the region of frontal cortex is related with the hormone modulated [29], and it shows more stability of alpha brain activity with this reaction.

In this thesis we lay stress on the method development, we provide a method for the detection of transient EEG activity. So far we don't have important discovery of results on these subjects, but we obtained suitable section of long-term signal for the microstate analysis, and it is useful for future researches of transient phenomenon.

4.2 Future Work

Brain microstate analysis can be extended to the exploration of other EEG features. Although current study was focused on alpha dipolar-vector model, it is an important and appealing issue on the variations of alpha rhythmic compositions based on multi-resolution spectral analysis. The phenomenon might be correlated with brain oscillatory model of alpha rhythms. Then, the further step may be taken to investigate the spatio-spectral microstate of alpha brain either during Zen meditation or at normal relaxation.

References

- [1] T. Kalayci and Ö. Özdamar, “Wavelet preprocessing for automated neural network detection of EEG spikes,” *IEEE Eng. Med. Biol. M.*, vol. 14, no. 2, pp. 160–166, 1995.
- [2] R. Cooper, J. W. Osselton, and J. C. Shaw, *EEG Technology*, 3rd ed. Woburn, MA: Butterworth, 1980.
- [3] K. Ansari-Asl, J.J. Bellanger, F. Bartolomei, F. Wendling and L. Senhadji, “Time-Frequency Characterization of Interdependencies in Nonstationary Signals: Application to Epileptic EEG,” *IEEE Transactions on Biomedical Engineering*, vol. 52, no. 7, pp. 1218-1226, Jul. 2005.
- [4] N. Acir and M. Kuntalp, “Automatic Detection of Epileptiform Events in EEG by a Three-Stage procedure Based on Artificial Neural Networks,” *IEEE Transactions on Biomedical Engineering*, vol. 52, no. 1, pp. 30-40, Jan. 2005.
- [5] E.ST. Louis and E. Lansky, “Meditation and epilepsy: A still hung jury,” *Medical Hypotheses*, vol. 67, issue 2, pp. 247-250, Apr. 2006.
- [6] C. Babiloni, G. Frisoni and M. Steriade, “Frontal white matter volume and delta EEG sources negatively correlate in awake subjects with mild cognitive impairment and Alzheimer's disease,” *Clinical Neurophysiology*, vol. 117, pp. 1113–1129, Jan. 2006.
- [7] O.L. Carter, D.E. Presti and C. callistmon, “Meditation alters perceptual rivalry in Tibetan Buddhist monks,” *Current Biology*, vol. 15, no.11, pp. 412-413, 2005.
- [8] S.W. Lazar, C.E. Kerr and R.H. Wassermana, “Meditation experience is associated with increased cortical thickness,” *Neuroreport*, vol. 16, no. 17, pp.1893–1897, Nov. 2005.
- [9] D.A. Lindberg, “Integrative Review of Research Related to Meditation, Spirituality, and the Elderly,” *Geriatric Nursing*, vol. 26, no. 6, 2005.

- [10] R.C. Shetty, "Meditation and its implications in non pharmacological management of stress related emotions and cognitions," *medical hypotheses*, pp. 1198-1199, 2005.
- [11] M.J. Ott and Rebecca L. Norris, "Mindfulness Meditation for Oncology Patients: A Discussion and Critical Review," *Integr Cancer Therapies*, vol. 5, no. 2, pp. 98-108, 2006.
- [12] L.S. John, *Biosignal and Biomedical Image Processing*. MARCEL DEKKER , 2004, pp. 149.
- [13] I. Daubechies, *Ten lectures on wavelets*. Philadelphia, PA: SIAM, 1992.
- [14] A.R. de Leona and K.C. Carrière, "A generalized Mahalanobis distance for mixed data," *Journal of Multivariate Analysis*, vol. 92, issue 1, pp. 174-185, Jan. 2005.
- [15] R.D. Maesschalck, D.J. Rimbaud and D.L. Massart, "The Mahalanobis distance," *Chemometrics and Intelligent Laboratory Systems*, vol. 50, Issue 1, pp. 1-18, Jan. 2000.
- [16] D. Lehmann and T. Koenig, "Spatio-temporal dynamics of alpha brain electric fields, and cognitive modes," *International Journal of Psychophysiology*, vol. 26, pp. 99-112, 1997.
- [17] D. Lehmann, "Multichannel topography of human alpha EEG fields," *Electroencephalogr Clin Neurophysiol*, vol. 31, no. 5, pp. 439-49, Nov. 1971.
- [18] J.L. Cantero, M. Atienza, R.M. Salas and C. Gomez, "Brain Spatial Microstates of Human Spontaneous Alpha Activity in Related Wakefulness, Drowsiness Period, and REM Sleep," *Brain Topography*, vol. 11, no. 4, pp. 257-263, Jun. 1999.
- [19] B. S. Oken and K.H. Chiappa, "Statistical issues concerning computerized analysis of brainwave topography," *Annals of Neurology*, vol. 19, issue 5, pp. 493-497, May 1986.

- [20] SE. Lukas, JH. Mendelson, BT. Woods, NK. Mello and SK. Teoh, "Topographic distribution of EEG alpha activity during ethanol-induced intoxication in women," *Journals of Studies on Alcohol*, vol. 50, pp. 176-85, Mar. 1989.
- [21] J. Zeitlhofer, P. Anderer, S. Obergottsberger, P. Schimicek, S. Lurger, E. Marschnigg, B. Saletu and L. Deecke1, "Topographic mapping of EEG during sleep," *Springer Netherland*, vol. 6, no. 2, pp. 123-129, Mar. 1993.
- [22] J.L. Cantero, M. Atienza, C. Gomez, "Spectral Structure and Brain Mapping of Human Alpha Activities in Different Arousal States," *Neuropsychobiology*, vol. 39, pp. 110-116, 1999.
- [23] G. Bush, P. Luu and M.I Posner., "Cognitive and emotional influences in anterior cingulate cortex," *Trends in Cognitive Sciences*, vol. 4, pp. 215-222, 2000.
- [24] C.R. Maclean, K.G. Walton, S.R. Wenneberg, D.K Levitsky, J.P. Mandarino, R. Waziri, S.L. Hills, R.H. Schneider, "Effect of the Transcendental Meditation program on adaptive mechanisms: changes in hormone levels and responses to stress after 4 months of practice," *Psychoneuroendocrinology*, vol. 22, pp. 277-295, 1997.
- [25] D.N. Pandya and B. Seltzer, "Association areas of cerebral cortex," *Trends in Neuroscience*, vol. 5, pp. 386-390, 1982.
- [26] J. Wu, M.S. Buchsbaum, J.C. Gillin, C. Tang, S. Cadwell, M. Wiegand, A. Najafi, E. Klein, K. Hazen, W.J Bunney, J.H. Fallon and D. Keator, "Prediction of antidepressant effect of sleep deprivation by metabolic rates in the ventral anterior cingulated and medial prefrontal cortex," *The American Journal of Psychiatry*, vol. 156, pp. 1149-1158, 1999.
- [27] K.L. Phan, S.F. Taylor, R.C. Welsh, L.R. decker, D.C. Noll, T.E. Nichols, J.C. Britton, I. Liberzon, "Active of the medial prefrontal cortex and extended amygdale by individual ratings of emotional arousal: a fMRI study," *Biological Psychiatry*, vol. 53, pp. 211-215, 2003.
- [28] K.N. Ochsner, J.J. Gross, "The cognitive control of emotion," *Trends in Cognitive Sciences*, vol. 9, pp. 242-249, 2005.

- [29] S. Yamamoto, Y. Kitamura, N. Yamada, Y. Nakashima, S. Kuroda, “Medial Prefrontal Cortex and Anterior Cingulate Cortex in the Generation of Alpha Activity Induced by Transcendental Meditation: A Magnetoencephalographic Study, *Acta Medica Okayama*,” vol. 60, no. 1, 2006.



Appendixes

A.1 Discrete Wavelet Transform

Wavelets are mathematical formulae that decompose data into components with different resolutions quantified by the so-called scale. The advantages of wavelet analysis over traditional Fourier methods are mainly the capability of analyzing signal with time-varying, multi-resolution behaviors. Wavelets were developed independently in the fields of mathematics, quantum physics, electrical engineering, seismic geology, etc. The wavelet can be characterized by a wave which is bounded with zero average in a limit time range. The wavelet transform then allows us to construct a time-frequency relationship, which showed the time-varying frequency components.

Consider a real or complex continuous function $\psi(t)$ as the *mother wavelet* or simply *wavelet*. It possesses the characteristics of zero integration and bounded waveform pattern. The property of zero integration implies that the function $\psi(t)$ has ripples, while the property of bounded waveform means the energy of function $\psi(t)$ is bounded in a limited time range. The area of function $\psi(t)$ should be small, and its amplitude reduces to zero rapidly towards two ends of the waveform.

A set of continuous wavelet functions can be derived by scaling (expanding or contracting)

as well as shifting the mother wavelet function $\psi(t)$. as follows

$$\psi_{a,b}(t) = \frac{1}{\sqrt{a}} \psi\left(\frac{t-b}{a}\right), \quad (\text{A.1})$$

In the above equation, a is a positive real parameter defining the scale and b is a real indicating the time shift. The continuous wavelet transform cannot be implemented for digital signals. Concept and approach for discrete wavelet transform have thus been developed for digital realization and implementation. We modify the parameters a, b as $a = a_0^m$ and $b = n$, respectively, where $m, n \in Z$ integer, $a_0 \neq 1$. When $a_0 = 2$, then the wavelet is called the

“Dyadic Wavelet”, and Eq. (2.1) becomes

$$\psi_{m,n}(k) = \frac{1}{\sqrt{2^m}} \psi\left(\frac{k-n}{2^m}\right). \quad (\text{A.2})$$

Therefore, the discrete wavelet transform $DWT_f(m, n)$ is defined below

$$DWT_f(m, n) = \frac{1}{\sqrt{2^m}} \sum_k f(k) \psi^*\left(\frac{k-n}{2^m}\right). \quad (\text{A.3})$$

where the discrete wavelet transform $DWT_f(m, n)$ was a function of signal $f(k)$, and k was a operation index.

The discrete wavelet transform is applied to the decomposition of a signal which had into the high-frequency components and low frequency components. By the orthogonal wavelet basis functions, the input signal $x(k)$ is decomposed as

$$x(n) = \sum_k cA_i(k) \phi_{j-i,k}(n) + \sum_k cD_i(k) w_{j-i,k}(n) + \dots + \sum_k cD_1(k) w_{j-1,k}(n), \quad (\text{A.4})$$

where the scaling function $\phi_{j,k}(n)$ is defined as:

$$\phi_{j,k}(n) = \sqrt{2^j} \phi(2^j n - k) \quad (\text{A.5})$$

and the wavelet function

$$w_{j,k}(n) = \sqrt{2^j} w(2^j n - k). \quad (\text{A.6})$$

cA_i and cD_i are the coefficients corresponded to the basis functions, i represented the level of the transformation. The relationship between of discrete wavelet transform and inverse discrete wavelet transform of single level is

DWT:

$$cA_{i+1}(k) = \sum_n h_0(n-2k) cA_i(n) \quad \text{and} \quad (\text{A.7})$$

$$cD_{i+1}(k) = \sum_n h_1(n-2k) cA_i(n). \quad (\text{A.8})$$

IDWT:

$$cA_i(n) = \sum_k cA_{i+1}(k) h_0(n-2k) + \sum_k cD_{i+1}(k) h_1(n-2k). \quad (\text{A.9})$$

The $h_0(n)$ and $h_1(n)$ are the filters and the relationship between scaling function and wavelet function as follow:

$$\phi(n) = \sum_k h_0(k) \sqrt{2} \phi(2n-k) \quad \text{and} \quad (\text{A.10})$$

$$w(n) = \sum_k h_1(k) \sqrt{2} \phi(2n-k). \quad (\text{A.11})$$

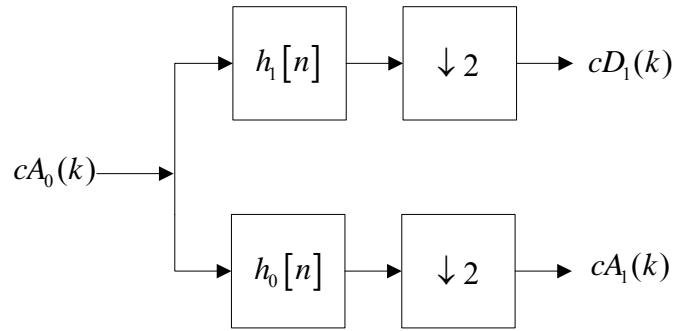


Figure A.1 Discrete Wavelet Decomposition

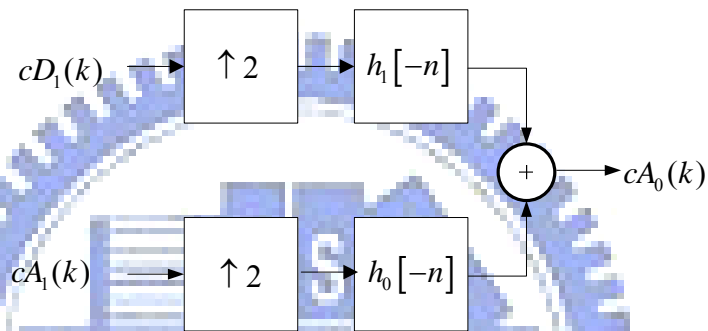


Figure A.2 Discrete Wavelet Reconstruction

Figure A.1 shows the Discrete Wavelet Decomposition process. The signal respectively passes through the high-pass and low-pass filters and then is down sampled by 2. We obtain the frequency component of the signal by this process for further analysis. Fig A.2 shows the process of Discrete Wavelet Reconstruction during which the decomposed signal is up-sampled and pass through the filters. By the decomposition and reconstruction, we could obtain a signal that has particular frequency component that we need, and in this thesis we used Daubechies 6 as the filters. In EEG signal, the most we concern about is alpha wave (8~12Hz). Figure A.3 shows that if the signal is 1000 Hz sampling, we could obtain the alpha

wave of the signal by the level 6 Wavelet Decomposition.

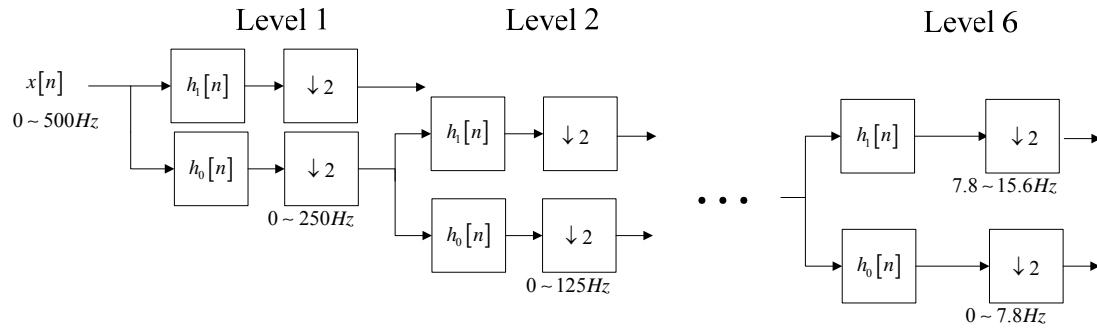


Figure A.3 Extraction the alpha wave by the Wavelet Decomposition.

A.2 Mahalanobis Distance

In the case of object- i with two variables $x_i = (\mu_{i1}, \mu_{i2})$, the ED with regard to the center of data can be calculated for each object. Assume totally N objects, ED for object- i is computed as

$$ED_i = \sqrt{(\mu_{i1} - \bar{\mu}_1)^2 + (\mu_{i2} - \bar{\mu}_2)^2} \quad \text{for } i = 1 \text{ to } N, \quad (\text{A.12})$$

Where μ_{i1} and μ_{i2} are the variables of object- i , $\bar{\mu}_1$ and $\bar{\mu}_2$ are the means of two variables of total n objects.

To be able to compute the MD, first the variance-covariance matrix C_x is calculated:

$$C_x = \frac{1}{(N-1)} (X_c)^T (X_c), \quad (\text{A.13})$$

where the X is the data matrix containing N objects in the rows, X_c is the data matrix

X subtracted by the variable means \bar{X} ; $X_c = (X - \bar{X})$. In the case of two variables, μ_{i1}

and μ_{i2} , the variance-covariance matrix is

$$C_x = \begin{bmatrix} \sigma_1^2 & \rho_{12}\sigma_1\sigma_2 \\ \rho_{12}\sigma_1\sigma_2 & \sigma_2^2 \end{bmatrix}, \quad (\text{A.14})$$

where σ_1^2 and σ_2^2 are the variances of the first and second variables, respectively and

$\rho_{12} = \sqrt{1 - \frac{\det(C_x)}{\sigma_1^2\sigma_2^2}}$; while $\rho_{12}\sigma_1\sigma_2$ is the covariance between the two variables.

The MD for object- i χ_i is then

$$MD_i = \sqrt{(x_i - \bar{x})C_x^{-1}(x_i - \bar{x})^T} \quad (\text{A.15})$$

where \bar{x} is the center of the data.

with

$$C_x^{-1} = \begin{bmatrix} \sigma_2^2/\det(C_x) & -\rho_{12}\sigma_1\sigma_2/\det(C_x) \\ -\rho_{12}\sigma_1\sigma_2/\det(C_x) & \sigma_1^2/\det(C_x) \end{bmatrix},$$

where $\det(C_x) = \sigma_1^2\sigma_2^2(1 - \rho_{12}^2)$ is the determinant of the variance-covariance matrix.

For an object- i x_i measured in two variables, μ_{i1} and μ_{i2} , Eq. (A.15) could be

rewritten, since

$$\left[(\mu_{i1} - \bar{\mu}_1)(\mu_{i2} - \bar{\mu}_2) \right] C_x^{-1} = \left[\frac{\sigma_2^2(\mu_{i1} - \bar{\mu}_1) - (\mu_{i2} - \bar{\mu}_2)\rho_{12}\sigma_1\sigma_2}{\det(C_x)} \quad \frac{\sigma_1^2(\mu_{i2} - \bar{\mu}_2) - (\mu_{i1} - \bar{\mu}_1)\rho_{12}\sigma_1\sigma_2}{\det(C_x)} \right]$$

and

$$\left[(\mu_{i1} - \bar{\mu}_1)(\mu_{i2} - \bar{\mu}_2) \right] C_x^{-1} \begin{bmatrix} (\mu_{i1} - \bar{\mu}_1) \\ (\mu_{i2} - \bar{\mu}_2) \end{bmatrix}$$

$$\begin{aligned}
&= \frac{\sigma_2^2 (\mu_{i1} - \bar{\mu}_1)^2 - (\mu_{i2} - \bar{\mu}_2)(\mu_{i1} - \bar{\mu}_1) \rho_{12} \sigma_1 \sigma_2}{\det(C_x)} \frac{\sigma_1^2 (\mu_{i2} - \bar{\mu}_2)^2 - (\mu_{i1} - \bar{\mu}_1)(\mu_{i2} - \bar{\mu}_2) \rho_{12} \sigma_1 \sigma_2}{\det(C_x)} \\
&= \frac{\sigma_2^2 (\mu_{i1} - \bar{\mu}_1)^2 (1 - \rho_{12}^2) + \sigma_1^2 (\mu_{i2} - \bar{\mu}_2)^2 - 2 (\mu_{i1} - \bar{\mu}_1)(\mu_{i2} - \bar{\mu}_2) \rho_{12} \sigma_1 \sigma_2 + \sigma_2^2 (\mu_{i1} - \bar{\mu}_1) \rho_{12}^2}{\sigma_1^2 \sigma_2^2 (1 - \rho_{12}^2)} \\
&= \frac{(\mu_{i1} - \bar{\mu}_1)^2}{\sigma_1^2} + \frac{(\mu_{i2} - \bar{\mu}_2)^2}{\sigma_2^2 (1 - \rho_{12}^2)} - 2 \frac{(\mu_{i1} - \bar{\mu}_1)(\mu_{i2} - \bar{\mu}_2) \rho_{12}}{\sigma_1^2 \sigma_2^2 (1 - \rho_{12}^2)} + \frac{\rho_{12}^2 (\mu_{i1} - \bar{\mu}_1)^2}{\sigma_1^2 (1 - \rho_{12}^2)} \\
&= \frac{(\mu_{i1} - \bar{\mu}_1)^2}{\sigma_1^2} + \left(\frac{\mu_{i2} - \bar{\mu}_2}{\sigma_2 \sqrt{1 - \rho_{12}^2}} - \frac{\mu_{i1} - \bar{\mu}_1}{\sigma_1 \sqrt{1 - \rho_{12}^2}} \right)^2
\end{aligned}$$

so that

$$MD_i = \sqrt{\frac{(\mu_{i1} - \bar{\mu}_1)^2}{\sigma_1^2} + \left[\left(\frac{\mu_{i2} - \bar{\mu}_2}{\sigma_2} - \rho_{12} \left(\frac{\mu_{i1} - \bar{\mu}_1}{\sigma_1} \right) \right) \frac{1}{\sqrt{1 - \rho_{12}^2}} \right]^2} \quad (\text{A.16})$$

This expression shows that the part of second variable which is already explained by the first variable is subtracted. In other words, the MD adjusts itself to the correlation within the data. When x_{i1} and x_{i2} are uncorrelated ($\rho_{12} = 0$), equation (A.16) is reduced to the formula for the ED in Eq. (A.12).